Finite temperature topological order in 2D topological color codes

Mehdi Kargarian*
Physics Department, Sharif University of Technology, Tehran 11155-9161, Iran
(Dated: July 19, 2009)

In this work the topological order at finite temperature in two-dimensional color code is studied. The topological entropy is used to measure the behavior of the topological order. Topological order in color code arises from the colored string-net structures. By imposing the hard constrained limit the exact solution of the entanglement entropy becomes possible. For finite size systems, by rising the temperature one type of string-net structures is thermalized and the associative topological entropy vanishes. In the thermodynamic limit the underlying topological order is fragile even at very low temperatures. Taking first thermodynamic limit and then zero-temperature limit and vice versa don't commute, and their difference is related only to the topology of regions. The contribution of the colors and symmetry of the model in the topological entropy is also discussed. It is shown how the gauge symmetry of the color code underlies the topological entropy.

PACS numbers: 03.67.Lx, 03.67.Mn, 03.65.Ud

arXiv:0904.4492v2 [quant-ph] 19 Jul 2009

I. INTRODUCTION

Exotic sates of matter are those that defy the usual description in terms of well-known Landau-Ginzburg-Wilson paradigm[1], where an appropriate local order parameter characterizes different behaviors of two phases on either side of the critical point. These are new phases of matter carrying a kind of quantum order called *topological order*[2] and the transition between various phases does not depend on the symmetry breaking mechanism. From the experimental point of view, the fractional quantum Hall liquids[3,4,5] exhibits topological order. Different phases of electron liquids carry the same symmetry and the phase transition between them is possible. Therefore, the Landau theory of classical phase transitions fails in order to describe these phases. The most remarkable properties of such new states are the dependency of the ground state degeneracy on genus or handles of the space, gapped excitations and non-trivial braiding of excitations. This latter property introduces new class of emerging particles with the statistical properties that are neither fermions nor bosons. In fact, they are *anyons*. They interact topologically independent of their distances much like that of Aharonov-Bohm interaction. If by winding of an anyon around another one the wavefunction picks up an overall phase, the anyons are called *abelian* anyons. But, if evolution of the wavefunction is captured by a unitary matrix, the anyons are called *non-abelian* anyons, i.e. they obey non-abelian braiding statistics.

The questions such as what the objects underlying the topological phases are and how different phases can be classified are still under debate. However, some physical mechanisms such as string/membrane-net condensation[6,7], branyons[8] that are analogous of the particle condensation in the symmetry-breaking phases and a description in terms of quantum groups[9] have been introduced. The string-nets are extended nonlocal objects and the ground state is a coherent superposition of all possible string's configurations appearing at all length scale. This physical picture clarifies the topological order based on the microscopic degrees of freedom. Emerging particles such as fermions or anyons are collective excitations of strings[10].

The fact that in topological ordered phases the ground state subspace has a robust degeneracy and the excitations above the ground state are gapped give them the ability of being rigorous quantum memory[11] in the sense of error correction. However, these are not sufficient conditions for being self-correcting code. Perhaps thermal noises spoil the self-stability of the code[12,13]. The construction of fault-tolerant topological quantum computation[14] exploits the emerging properties of topological ordered phases. The quantum information can be stored on the topologically protected subspace being free from the decoherence. The robust manipulation of quantum information is done by braiding of anyons[15,16,17,18], where the unitary gate operations are carried out by braiding of anyons.

The ground state of topological ordered phases is highly entangled state and an indicator for topological order which is not based on symmetry has been emerged, notably the topological entanglement entropy[19,20]. This topological quantity appears as subleading correction to the entanglement entropy of a convex region. It is a general feature of all gapped phases that the entanglement entropy scales with the boundary of the region, the so called *area law*[21]. However, the appearance of constant subleading term is a new feature related to topological order. The topological phase can be described as a phase of matter for which the low-energy effective theory is a topological field theory (TQFT). Topological entanglement entropy is related to one of the basic parameter of the TQFT, the total quantum dimension of emerging quasiparticles in the theory.

The best known model for studying topological order, emerging abelian or non-abelian anyons and examining its capabilities for topological quantum computations is the famous Kitaev's model[22]. In the abelian phase, the model becomes the well-known toric code with a stabi-

lizer structure[23]. The stabilizer structure of the code is given by a set of *star* and *plaquette* operators. Stabilizer operators fix a subspace in the Hilbert space of the model in which different states are distinguished by means of topological numbers. *Topological color code* is another relevant example of stabilizer codes, with enhanced computational capabilities[24,25]. The stabilizer operators are only colored plaquette operators. However, both codes are topological because the stabilizer operators are local and non-detectable errors have non-trivial supports on the manifold. Non-trivial string operators stand for encoded logical operators. Topological order in toric code and color code are related to different gauge symmetry. Indeed, the topological order in the toric code is related to the $\mathbf{Z_2}$ gauge symmetry, whereas the topological order in the color code is related to the $\mathbf{Z_2} \times \mathbf{Z_2}$ gauge symmetry. This latter symmetry arises from the contribution of the colors in the construction of the code and is responsible of the string-net structure of the code. However, both models have almost the same error threshold when one considers the error syndrome measurements[26].

Entanglement properties of both models at zero-temperature have been extensively studied. The entanglement entropy of a region with its complement depends on the degrees of freedom living on the boundary of the region supplemented with a topological term. But, the topological term for the color code[27] is just twice than the toric code[28] when both lattices are put on a compact surface. The difference arises because the excitations in the toric code are ascribed to the four superselection sectors, whereas the contribution of the colors in the color code model makes the excitations richer than those of the toric code. In fact in the color code the number of superselection sectors is sixteen.

How much topological order is robust against the thermal fluctuations? This is a very important question from the practical point of view since every practical implementation of quantum information processing can not ignore the effects of thermal fluctuations. Thermal fluctuations may create excitations (errors) accumulating in the system and destroying the quantum information encoded in the states. Original idea of topological order which is a zero temperature concept can be extended to thermal mixed states[29], where classical limit arises by washing out the off diagonal elements of the density matrix. With such realization of classical topological order, it would be tempted to investigate the topological order in terms of temperature. It can be used as a measure of resilience of a code against the temperature. We would like to point out at finite temperature the entanglement entropy is no longer a measure of correlations between subsystems. Instead, the mutual information does as it scales with the boundary of subsystems. The topological order however manifests itself as subleading terms of entanglement entropy as well as mutual information. As long as we are interested in the topological order, a linear combination of entropies or mutual information[30] of subsystems gives a measure of topological order, since in the combination the dependency on bulk and boundary degrees of freedom are washed out. In the toric code each of its underlying loop structure or gauge structure contributes exactly half to the topological entanglement entropy. This is expected since both loop structures are similar in a fashion that they are defined on the original lattice and its dual. For a finite size system topological order survives even at non-zero temperatures[30,31]. Further increasing of temperature destroys the loop structures of the model implying the fragility of the toric code[12,32,33].

In this work we address the above problem, i.e the fate of topological order at finite temperature, in the color codes. The loop structures of the color code is different from that of toric code since they are related to different gauge symmetries. We discuss how gauge symmetry affects the finite temperature properties of the code. We attach to each set of plaquettes with the same color an energy scale. In the lattice gauge theory these energy scales are translated into the chemical potential for creating the respective charges. Following the derivation of C. Castelnovo, *et al*[31], we first impose the hard constrained limit on the string-net structure in σ^z bases and allow for the thermalization of the string-net structure in σ^x bases. Then, in order to identify the contribution of colored strings in the topological entanglement entropy, we fix other loop structures and examine the residual topological order. Also in the high temperature limit the description in terms of classical topological order is recovered.

The organization of the paper is as follows. In the next section the color codes is briefly reviewed. Then in Sec(III) the thermal density matrix that is needed for subsequent arguments is derived. In Sec(IV) the entanglement entropy is derived from the density matrix. Then, limiting behavior of the entanglement is discussed in Sec(V). Topological entanglement entropy and its behavior in terms of temperature is the subject of Sec(VI). The case of open boundary conditions is discussed in Sec(VII). Sec(VIII) is devoted to conclusions.

II. 2-COLEX AND COLOR CODE: FIXING NOTATIONS

Let us start by a brief introductory on the color code model. Consider a two-dimensional trivalent lattice composed of plaquettes, vertices and links. Such structure is shown in Fig.1. To keep track of vertices, plaquettes and links, we use color as a bookkeeping tool. We will use three colors: red, green and blue. Then we color the plaquettes of the lattice in which two neighboring plaquettes don't share in the same color. In this way we can also color links so that a c-link (the letter c stand for color throughout the paper unless stated another meaning) connects two c-plaquettes. We call this two-dimensional lattice a *2-colex*. The lattice can also be embedded in higher spatial dimensions, the so-called D-

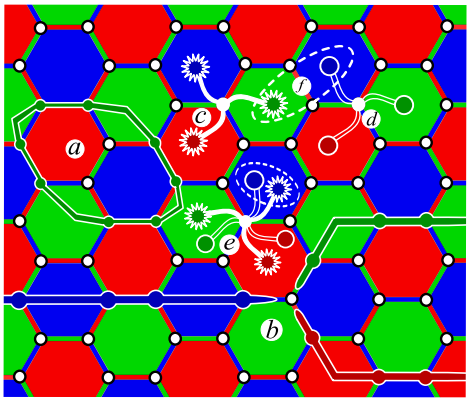

FIG. 1: (color online) A piece of 2-colex with colored hexagons as its plaquettes. Lightest to darkest hexagons: green, red and blue, respectively (a) The closed green string corresponds to the product of blue and red plaquettes. (b) A generalization of the closed colored strings, the string-net. (c) Performing a σ^z rotation creates excitations with topological charges (e, χ_c) (d) σ^x rotation creates other types of excitations with charges (c, χ_e) (e) σ^y rotation creates both types of quasiparticles at corresponding plaquettes. The composite particle in the dashed ellipse is a boson with charge (b, χ_b) (f) The composite particle in the dashed ellipse is a fermion with charge (b, χ_g).

colex[8,34]. Hence, the thermal analysis presented here can be extended to higher dimensional cases as in the toric code[35]. Without loss of generality we suppose all plaquettes are hexagons. Suppose the 2-colex is embedded on a compact surface such as torus, i.e imposing periodic boundary conditions. To connect the lattice to a physical system, we place a qubit at each vertex . With each plaquette we attach two operators aimed at reaching the stabilizer code. These operators are simply the product of a set Pauli operators acting on the qubits around a c-plaquette: $X_c = \prod_{i\in\partial P} \sigma_i^x$ and $Z_c = \prod_{i\in\partial P} \sigma_i^z$, where ∂P stands for six qubits around a c-plaquette. With this definition for plaquette operators we see that all plaquettes of either color are treated on equal footing. Although the colors play no role in the plaquette operators, they determine the structure of the coding space. It is simple to see that all plaquette operators commute with each other since they share either nothing or at even number of qubits. The plaquette operators are generators of a stabilizer group; thereby there are vectors in a subspace of the whole Hilbert space that are common eigenvectors of all plaquette operators with eigenvalue $+1$. This subspace, the coding space, is spanned by some vectors that are distinguished by eigenvalues of a set of non-local operators in which their supports wind the handles of the space[24,27]. Although three distinct colors introduce the code, there is an interplay between color and homology of the space. In fact for each homology class only two colors are independent related to the symmetry of the code. As long as we consider closed spaces such as torus, the closed non-contractible loops are enough to form bases for the coding space. The coding space is called *color code*. From now on, unless it is stated else, we suppose the 2-colex spanned by $3N$ plaquettes, N of each color. Notice that on a compact surface like a torus all plaquette operators are not independent. In fact they are subject to the constraint $\prod_{g\in\mathcal{G}} \Omega_g = \prod_{b\in\mathcal{B}} \Omega_b = \prod_{r\in\mathcal{R}} \Omega_r$, where $\Omega = X, Z$, and $\mathcal{G}$, $\mathcal{B}$, $\mathcal{R}$ are sets of green, blue and red plaquettes, respectively.

The protected subspace is ground state of a many-body Hamiltonian that is minus sum of all plaquette operators equipped with some coupling constants as follows:

$$\begin{aligned} H \;=\; & -\lambda_x^g \sum_{g\in\mathcal{G}} X_g - \lambda_x^b \sum_{b\in\mathcal{B}} X_b - \lambda_x^r \sum_{r\in\mathcal{R}} X_r \\ & -\lambda_z^g \sum_{g\in\mathcal{G}} Z_g - \lambda_z^b \sum_{b\in\mathcal{B}} Z_b - \lambda_z^r \sum_{r\in\mathcal{R}} Z_r, \end{aligned} \qquad (1)$$

where $\lambda_{x,z}^c$'s are coupling constants and each sum runs over all corresponding c-plaquettes. The ground states spanning the coding space are all vectors in which $X_c|\psi\rangle = Z_c|\psi\rangle = |\psi\rangle$ for all plaquette operators. Any violation of this condition amounts to an excited state or alternatively as an *error*. Therefore, the ground state is said to be vortex free in the sense of being closed string-net condensate. In fact, the ground state is an equal weighted superposition of all string-net configurations. Such configurations can be visualized if we consider the product of plaquette operators. For example consider the product of two neighboring red and blue plaquettes. In the product, the Pauli operators of qubits shared between two plaquettes square identity and we are left with a green string being boundary of two plaquettes. This closed green string has been shown in Fig.1(a), which connects green plaquettes. Such closed strings of either size and color commute with Hamiltonian. Another interesting extended object underlying the ground state structure is string-net that is a collection of colored strings. A typical string-net has been depicted in Fig.1(b). The associated string-net operator can be the product of either σ^x or σ^z acting on the qubits it contains (filled colored circles on the string-net). This string operator commutes with all plaquettes since they share either nothing or even number of qubits. The appearance of such string-net is crucial for the full implementation of the Clifford group[24].

Excitations appear as end points of open colored strings. An open string anticommutes with the plaquettes lying at its ends as they share odd number of qubits. To have a simple picture of excitations, let us focus on some simple cases. Consider a rotation σ^z applied to a certain qubit as in Fig.1(c). As σ^z anticommutes with X_r, X_b and X_g plaquette operators adjacent to the qubit, it will increase the energy of plaquettes by $2\lambda_x^r$, $2\lambda_x^b$ and $2\lambda_x^g$, respectively. In this case the excitation on

a c-plaquette is revealed by an c-star. Similarly, if we perform a σ^x rotation on a qubit as in Fig.1(d), the anticommutation of σ^x with Z_c of neighboring plaquettes leads the energy of red, blue and green plaquettes increase by $2\lambda_z^r$, $2\lambda_z^b$ and $2\lambda_z^g$, respectively. In this case the excitation on a c-plaquette is revealed by a c-circle. If a rotation σ^y is performed, as in Fig.(1e), each plaquette contains both above excitations, i.e. the excitations on the c-plaquette increase the energy by $2\lambda_x^c + 2\lambda_z^c$. All quasiparticles are by themselves boson. However, they may have mutual semionic statistics. For instance, if a red particle of Fig.(1d) go around a green particle of Fig.(1c) , the wavefunction picks up a minus sign implying they are anyons. There are also composite particles of two excitations as shown by white dashed ellipses. If two excitations differ in both color and type, they form a fermion as in Fig.1(f). Otherwise, they form a boson as in Fig.1(e).

All above emerging particles that are the low energy excitations of the model can be classified in terms of underlying gauge group[36,37]. Before that, let us make a convention for colors which will be useful for subsequent discussions. We refer to colors by a bar operation $\bar{c}$ that transform colors cyclically as $\bar{r} = g$, $\bar{g} = b$ and $\bar{b} = r$. The elements of the gauge group $\mathbf{Z_2} \times \mathbf{Z_2}$ are $\{e, r, b, g\}$. Each excitation carries a topological charge. The corresponding topological charge can be labeled by pair (q, χ), where $q \in \mathbf{Z_2} \times \mathbf{Z_2}$ and χ an irrp of this group. Therefore, there are nine bosons labeled by (c, χ_e), (e, χ_c) and (c, χ_c) and six fermions $(c, \chi_{\bar{c}})$ and $(c, \chi_{\bar{\bar{c}}})$. Taking into account the vacuum with trivial charge (e, χ_e), color code has sixteen topological charges or superselection sectors. Now, we can label the excitations in Fig.1 regarding their topological charges. The excitations in Fig.1(c) and Fig.1(d) have (e, χ_c) and (c, χ_e) charges, respectively, while the boson in Fig.1(e) and fermion in Fig.1(f) have (b, χ_b) and (b, χ_g) charges, respectively.

III. THERMAL DENSITY MATRIX OF COLOR CODE

Zero-temperature entanglement of the color code[27] is given by writing the ground state of the Hamiltonian in Eq.(1). Let G denotes the group constructed by a set of generators of the spin-flip plaquette operators, i.e X_c. By starting from a polarized state, the ground state will be an equal weighted superposition of all elements of the stabilizer group as follows.

$$|\psi\rangle = |G|^{-1/2} \sum_{h \in G} h|0\rangle^{\bigotimes |V|}, \tag{2}$$

where h is an element of the stabilizer group, $|G|$ is the cardinality of the group, $|V|$ is total number of vertices on the lattice and $\sigma^z|0\rangle = |0\rangle$. Other ground states can be constructed through the action of the non-local spin-flip operators with non-trivial supports winding the handles of the space. They are distinguished by different topological numbers. However, all of them have the same entanglement properties and we consider only one of them as above.

Topological order in the ground state of the color code Hamiltonian arises from the condensed string-net structures, which are loops without open ends. The ground state $|\psi\rangle$ has been written in the σ^z bases. In each term of the superposition a collection of spins related to the group element h have been flipped. Spins on the corresponding string-net have negative σ^z component. In this string-net structure $Z_c = 1$ for all plaquettes. There are also same string-net structures if we worked in the σ^x bases preserving the $X_c = 1$. This is because the model is symmetric upon the exchange of the σ^z and σ^x operators on the plaquettes. Unlike the toric code[31], both loop structures in the color code exist on the direct lattice since for each plaquette we attach two operators. The thermal fluctuations can break the string-nets and left them with open ends. That how much thermal effects are able to destroy the topological order associated to a string-net structure depends on the coupling constants in the Hamiltonian as well as size of the system. Definitely, we calculate the thermal density matrix and the topological entanglement entropy is used as a measure of topological order. Since the ground state is fixed point of all plaquette operators, its underlying topological order arises from coherent superposition of two string-net structures, each related to one of the bases. We impose a constraint in which the string-net structures related to the σ^z bases are preserved. The so called hard constrained limit[29] can be recasted into the limit $\lambda_z^c \to \infty$. One may expect that in this limit the thermal fluctuations can only create excitations with topological charges (e, χ_c). We can describe all excited states as $|\psi[\gamma^z]\rangle = \gamma^z|\psi\rangle$, where γ^z is any arbitrary product of σ^z Pauli operators. The density matrix $\rho = \exp(-\beta H)$ in the bases spanned by all states $|\psi[\gamma^z]\rangle$ is diagonal. However, things get more simplified if we work in the original bases $h|0\rangle^{\bigotimes |V|}$. Let us for simplicity drop the superscript $\bigotimes |V|$. In these bases the density matrix reads as follows

$$\rho = \frac{\sum_{h,\tilde{h} \in G} \langle 0|he^{-\beta H}h\tilde{h}|0\rangle h|0\rangle\langle 0|h\tilde{h}}{\sum_{h \in G}\langle 0|he^{-\beta H}h|0\rangle}. \tag{3}$$

Without loss of generality let $\lambda_z = \lambda_z^c$ for all plaquettes and $G_x = \sum_g X_g$, $B_x = \sum_b X_b$, $R_x = \sum_r X_r$ and $Z = \sum_c Z_c$. Then the Hamiltonian proposed in Eq.(1) can be written as

$$H = -\lambda_x^g G_x - \lambda_x^b B_x - \lambda_x^r R_x - \lambda_z Z. \tag{4}$$

Since $[Z, h] = 0$ for all h, then $Zh|0\rangle = 3Nh|0\rangle$ and the numerator of Eq.(3) reads as

$$\langle 0|he^{-\beta H}h\tilde{h}|0\rangle = e^{3\beta\lambda_z N}\langle 0|e^{\beta\lambda_x^g G_x + \beta\lambda_x^b B_x + \beta\lambda_x^r R_x}\tilde{h}|0\rangle. \tag{5}$$

Since each plaquette operator squares identity, i.e. $X_c^2 = 1$, each exponential term can be expressed in terms of

plaquette operators as follows.

$$e^{\beta\lambda_x^g G_x} = \prod_{g\in\mathcal{G}} \left[\cosh(\beta\lambda_x^g) + \sinh(\beta\lambda_x^g) X_g\right]. \tag{6}$$

The two remaining exponential terms $e^{\beta\lambda_x^b B_x}$ and $e^{\beta\lambda_x^r R_x}$ have the same expressions and obtained by replacing the color index g by b and r, respectively. Every element of the stabilizer group $\tilde{h}$ has a decomposition in terms of plaquette operators that it involves as $\tilde{h} = \prod_{g\in\tilde{h}} X_g \prod_{b\in\tilde{h}} X_b \prod_{r\in\tilde{h}} X_r$, where by $c \in \tilde{h}$ we imply if the c-plaquette operator exists in the decomposition of $\tilde{h}$. Let n_c be the number of c-plaquettes that exist in the decomposition of $\tilde{h}$. Hence, the only nonzero terms in Eq.(5) are as follows.

$$\langle 0|...|0\rangle = (\cosh\beta\lambda_x^g)^N (\cosh\beta\lambda_x^b)^N (\cosh\beta\lambda_x^r)^N \times \left[\sum_c e^{-(k_{\bar{c}}+k_{\bar{\bar{c}}})N - k_c n_c + k_{\bar{c}} n_{\bar{c}} + k_{\bar{\bar{c}}} n_{\bar{\bar{c}}}} + e^{-k_g n_g - k_b n_b - k_r n_r}\right], \tag{7}$$

where $k_c = -\ln(\tanh\beta\lambda_x^c)$ and the sum runs over three colors $c \in \{r, b, g\}$. Notice that the operator $\tilde{h}$ not only given by the product of green, blue and red plaquettes belonging to $\tilde{h}$ but also by other combinations of plaquettes due the periodic boundary conditions. In fact, the operator $\tilde{h}$ has the following expressions in terms of plaquettes operators.

$$\begin{aligned}
\tilde{h} &= \prod_{g\in\tilde{h}} X_g \prod_{b\in\tilde{h}} X_b \prod_{r\in\tilde{h}} X_r \\
&= \prod_{g\in\tilde{h}} X_g \prod_{b\in\mathcal{B}\setminus\tilde{h}} X_b \prod_{r\in\mathcal{R}\setminus\tilde{h}} X_r \\
&= \prod_{g\in\mathcal{G}\setminus\tilde{h}} X_g \prod_{b\in\tilde{h}} X_b \prod_{r\in\mathcal{R}\setminus\tilde{h}} X_r \\
&= \prod_{g\in\mathcal{G}\setminus\tilde{h}} X_g \prod_{b\in\mathcal{B}\setminus\tilde{h}} X_b \prod_{r\in\tilde{h}} X_r.
\end{aligned} \tag{8}$$

Note that in the above expressions by $c \in \mathcal{C}\setminus\tilde{h}$ we mean a c-plaquette in $\mathcal{C}$ ($\mathcal{C} = \mathcal{R}, \mathcal{G}, \mathcal{B}$) that is not in $\tilde{h}$. Now we can see that the ambiguity in Eq.(7) amounts to the above expressions for $\tilde{h}$. The partition function can be evaluated in a similar way as follows:

$$\mathcal{Z} = e^{3\beta\lambda_z N} (\cosh\beta\lambda_x^g)^N (\cosh\beta\lambda_x^b)^N \times (\cosh\beta\lambda_x^r)^N \left(1 + \sum_c e^{-(k_{\bar{c}}+k_{\bar{\bar{c}}})N}\right). \tag{9}$$

Thus, the density matrix can be recasted into the following form:

$$\rho = \frac{1}{|G|} \sum_{h,\tilde{h}\in G} \eta_T(\tilde{h}) \times h|0\rangle\langle 0|h\tilde{h}, \tag{10}$$

where

$$\eta_T(\tilde{h}) = \frac{\sum_c e^{-(k_{\bar{c}}+k_{\bar{\bar{c}}})N - k_c n_c + k_{\bar{c}} n_{\bar{c}} + k_{\bar{\bar{c}}} n_{\bar{\bar{c}}}} + e^{-k_g n_g - k_b n_b - k_r n_r}}{\sum_c e^{-(k_{\bar{c}}+k_{\bar{\bar{c}}})N} + 1}.$$

The limiting behavior of the density matrix at zero and very high temperatures is compatible with the respective known results. As temperature tends to zero ($k_c \to 0$), the pure density matrix $\rho = \frac{1}{|G|}\sum_{h,\tilde{h}} h|0\rangle\langle 0|h\tilde{h}$ is recovered[27]. At high-temperature limit, the totally mixed state $\rho = \frac{1}{|G|}\sum_h h|0\rangle\langle 0|h$ yields the classical limit of the model upon the hard constrained limit[29].

IV. ENTANGLEMENT ENTROPY

In order to calculate the entanglement entropy we consider a generic bipartition of the system into subsystems A and B. Notice that each bipartition may be composed of several disconnected regions. Suppose m_A and m_B stand for the number of respective bipartitions. Let Σ_A and Σ_B be the number of plaquette operators acting solely on A and B, respectively, and let Σ_{AB} stands for the number of plaquette operators acting simultaneously on A and B, i.e boundary operators. We focus on the entanglement entropy between two partitions A and B of the system. To this end, first the reduced density operator of the one subsystem is evaluated and then the entanglement entropy is measured using von Neumann entropy. The reduced density matrix of a region, say A, is obtained by tracing out ρ with respect to degrees of freedom of the subsystem B. Using the properties of the group[28], the reduced density matrix reads

$$\rho_A = \frac{1}{|G|} \sum_{h\in G, \tilde{h}\in G_A} \eta_T(\tilde{h}) h_A|0_A\rangle\langle_A 0|h_A\tilde{h}_A, \tag{11}$$

where G_A and G_B are subgroups of G which act trivially on subsystems B and A, respectively. The complete description of the subgroup G_A is given by a set of plaquette operators acting solely on A as well as collective operators. The latter is a collection of operators acting solely on A, but they are not the product of plaquettes in G_A. Suppose A is a simply connected region and the set $\{B_1, B_2, ..., B_{m_B}\}$ presents the disconnected components of B. Let AB_i be the collection of plaquette operators acting simultaneously on A and B_i. The product of c- and $\bar{c}$-plaquettes of component B_i with the c- and $\bar{c}$-plaquettes of the boundary AB_i produces a $\bar{\bar{c}}$-string acting solely on A. Denoting this string by $\gamma_i^{\bar{\bar{c}}}$, its expression will be

$$\gamma_i^{\bar{\bar{c}}} = \prod_{c,\bar{c}\in B_i\cup AB_i} X_c X_{\bar{c}}. \tag{12}$$

A schematic representation of these collective strings is shown in Fig.(2a). Therefore, for each disconnected

region we can realize three collective operators γ_i^r, γ_i^b and γ_i^g. For each disconnected region however only two of them are independent due to the local constraint $\gamma_i^r\gamma_i^b\gamma_i^g = 1$. There is also another constraint on the total number of collective operators. It is a global constraint: for a given color, say c, the product $\prod_i \gamma_i^c$ can be produced by product of all $\bar{c}$-and $\bar{\bar{c}}$-plaquettes acting solely on A, namely $\prod_i \gamma_i^c = \prod_{\bar{c},\bar{\bar{c}}\in A} X_{\bar{c}} X_{\bar{\bar{c}}}$. Taking into account all plaquettes, collective operators and constraints on them, the cardinality of the subgroups G_A and G_B will be $d_A = 2^{\Sigma_A+2m_B-2}$ and $d_B = 2^{\Sigma_B+2m_A-2}$, respectively.

The von Neumann entropy as a measure of entanglement between two bipartitions is given by $S_A = -\mathrm{Tr}(\rho_A \ln \rho_A)$. We don't use this relation to measure the entanglement. Here, we find it useful to instead compute it using the replica $S_A = \lim_{n\to 1} \partial_n \mathrm{Tr}[\rho_A^n]$. Hence, the trace of n-th power of the reduced density matrix will be[31]

$$\mathrm{Tr}[\rho_A^n] = \left(\frac{d_B}{|G|}\right)^{n-1} \prod_{l=1}^{n} \sum_{\tilde{h}_l \in G_A} \eta_T(\tilde{h}_l) \langle 0|\tilde{h}_{1,A}\tilde{h}_{2,A}...\tilde{h}_{n,A}|0\rangle. \tag{13}$$

In order to bring the above relation to a manageable form, we resort to a map between the group elements $\tilde{h}$ and the Ising variables[31]. Via this map the group elements are labeled by Ising variables based on which plaquettes and/or collective operators are involved in its expression. let $\theta_c = -1(+1)$ be a Ising variables related to appearing(not appearing) a c-plaquette in $\tilde{h}$. Similarly, $\Theta_i^c = -1(+1)$ related to appearing(not appearing) a collective c-string γ_i^c in $\tilde{h}$. Notice that this map is not a one-to-one map. In fact, it is a four-to-one map. This latter point arises from the fact that by considering three colors, if we reverse the sign of Ising variables related to two colors, they represent the same element in the group. This point is consistent with Eq.(8) and will be clear in following. The number of c-plaquettes, n_c, that the element $\tilde{h}$ involved can be expressed in terms of Ising variables as

$$n_c = \sum_{c\in\mathcal{C}} \frac{1-\theta_c}{2} + \sum_i (\Sigma_{B_i}^c + \Sigma_{AB_i}^c) \frac{1-\Theta_i^{\bar{c}}\Theta_i^{\bar{\bar{c}}}}{2}. \tag{14}$$

Here, Once the color index in n_c was fixed, the first sum runs over all c-plaquettes in $\mathcal{C}(\mathcal{G},\mathcal{B},\mathcal{R})$ and θ_c's take values of $-1(+1)$ as defined above accordingly, and the $\Sigma_{B_i}^c$ is the number of all c-plaquettes in B_i. let $\Sigma_{B_i}^c + \Sigma_{AB_i}^c = \Sigma_i^c$ and since $\Sigma_A^c + \sum_i \Sigma_i^c = N$, Eq.(14) can be written as

$$n_c = \frac{N}{2} - \frac{1}{2}\sum_{c\in\mathcal{C}} \theta_c - \frac{1}{2}\sum_i \Sigma_i^c \Theta_i^{\bar{c}}\Theta_i^{\bar{\bar{c}}}. \tag{15}$$

As we stated above, for a disconnected region B_i, the strings γ_i^r, γ_i^b and γ_i^g are not independent. With such dependency, the appearance of $\Theta_i^{\bar{c}}\Theta_i^{\bar{\bar{c}}}$ in above relation is meaningful. To see this, consider the case in which both $\bar{c}-$ and $\bar{\bar{c}}-$strings are present in the group element. This, in terms of Ising variables, yields $\Theta_i^{\bar{c}} = \Theta_i^{\bar{\bar{c}}} = -1$. But, the local constraint on strings implies that the product of two strings yield the $c-$string. Since there is not any c-plaquette in the decomposition of a c-string, the number of c-plaquettes arising from the collective operators will be zero.

In terms of Ising variables, the Eq.(13) will become

$$\mathrm{Tr}[\rho_A^n] = \left(\frac{d_B}{|G|}\right)^{n-1} \frac{1}{4^n} \prod_{l=1}^{n} \sum_{\{\theta_c^{(l)},\Theta_i^{(l)c}\}}^{const.} \eta_T\{\theta_c^{(l)},\Theta_i^{(l)c}\} \tag{16}$$

The coefficient $\frac{1}{4}$ comes form the $4-1$ mapping between Ising variables and plaquettes . The sum runs over all possible Ising variables subject to a constraint. This constraint arises by requiring the non-zero value for $\langle 0|\tilde{h}_{1,A}\tilde{h}_{2,A}...\tilde{h}_{n,A}|0\rangle$ in Eq.(13), which implies that the product of $\tilde{h}$'s must be trivial to give a non-zero value for the expectation value. The constraint can be applied by the following expression:

$$\sum_{I_r,I_b,I_g} \left\{ \prod_i \left[\delta\left(\prod_{l=1}^{n} \Theta_i^{(l)b}\Theta_i^{(l)g} - I_r\right) \delta\left(\prod_{l=1}^{n} \Theta_i^{(l)r}\Theta_i^{(l)g} - I_b\right) \delta\left(\prod_{l=1}^{n} \Theta_i^{(l)r}\Theta_i^{(l)b} - I_g\right) \right] \times \right.$$
$$\left. \prod_r \delta\left(\prod_{l=1}^{n} \theta_r^{(l)} - I_r\right) \prod_b \delta\left(\prod_{l=1}^{n} \theta_b^{(l)} - I_b\right) \prod_g \delta\left(\prod_{l=1}^{n} \theta_g^{(l)} - I_g\right) \right\} \delta\left(I_r I_b I_g - 1\right), \tag{17}$$

where $I_c = \pm 1$ subject to $I_r I_b I_g = 1$ which is imposed by the delta function in the second line of above expression. Notice that three delta functions in the first line are not independent and we could already drop one of them. However, we keep them to make the expression more symmetric. In fact, once two of them are fixed, the third one satisfied. This is just a reinterpretation of the local constraint that for a disconnected region only two strings are independent.

Regarding the map between Ising variables and pla-

quettes, we can fully bring the η_T in Eq.(10) into an expression in terms of Ising variables. Using Eq.(15), the η_T function reads as follows:

$$\eta_T = \frac{1}{4Z_0}\sum_{J_r,J_b,J_g}\left\{\prod_r e^{\frac{k_r}{2}J_r\theta_r}\prod_b e^{\frac{k_b}{2}J_b\theta_b}\prod_g e^{\frac{k_g}{2}J_g\theta_g}\prod_i e^{\frac{k_r}{2}J_r\Sigma_i^r\Theta_i^g\Theta_i^b+\frac{k_b}{2}J_b\Sigma_i^b\Theta_i^r\Theta_i^g+\frac{k_g}{2}J_g\Sigma_i^g\Theta_i^b\Theta_i^r}\right\}\delta(J_rJ_bJ_g-1), \quad (18)$$

where

$$Z_0 = \frac{1}{4}(e^{\frac{N}{2}(k_r+k_b+k_g)}+e^{\frac{N}{2}(k_r-k_b-k_g)}+ e^{\frac{N}{2}(-k_r+k_b-k_g)}+e^{\frac{N}{2}(-k_r-k_b+k_g)}),$$

and $J_c = \pm$ subject to $J_rJ_bJ_g = 1$ imposed by the delta function. Now we are in a position that we can rewrite the Eq.(16) in terms of Ising variables regarding to the constraint in Eq.(17). Also we use the fact that $\prod_{l=1}^n\sum_{J_c^l}F(J_c^l) = \sum_{\{J_c^l\}_{l=1}^n}\prod_{l=1}^n F(\{J_c^l\})$. Finally, we are left with the following expression.

$$\mathrm{Tr}[\rho_A^n] = \left(\frac{d_B}{|G|}\right)^{n-1}\frac{1}{4^{2n}Z_0^n}\sum_{\{J_c^l\}_{l=1}^n}{}'\sum_{I_c}{}'\left(\prod_r\sum_{\{\theta_r^l\}_{l=1}^n}^{\Delta_r=I_r}e^{\frac{k_r}{2}\sum_l J_r^l\theta_r^l}\right)\left(\prod_b\sum_{\{\theta_b^l\}_{l=1}^n}^{\Delta_b=I_b}e^{\frac{k_b}{2}\sum_l J_b^l\theta_b^l}\right)\left(\prod_g\sum_{\{\theta_g^l\}_{l=1}^n}^{\Delta_g=I_g}e^{\frac{k_g}{2}\sum_l J_g^l\theta_g^l}\right)\times$$
$$\left(\prod_i\sum_{\{\Theta_i^{(l)r,b,g}\}_{l=1}^n}^{\Delta_i^{c,\bar{c},\bar{\bar{c}}}=I_{c,\bar{c},\bar{\bar{c}}}}e^{\sum_l\left(\frac{k_r}{2}J_r^l\Sigma_i^r\Theta_i^{(l)g}\Theta_i^{(l)b}+\frac{k_b}{2}J_b^l\Sigma_i^{(l)b}\Theta_i^{(l)r}\Theta_i^{(l)g}+\frac{k_g}{2}J_g^l\Sigma_i^g\Theta_i^{(l)b}\Theta_i^{(l)r}\right)}\right), \quad (19)$$

where

$$\sum_{\{J_c^l\}_{l=1}^n}{}' \equiv \sum_{\{J_r^l\}_{l=1}^n}\sum_{\{J_b^l\}_{l=1}^n}\sum_{\{J_g^l\}_{l=1}^n}\prod_{l=1}^n\delta\left(J_r^lJ_b^lJ_g^l-1\right),$$
$$\sum_{I_c}{}' \equiv \sum_{I_r}\sum_{I_b}\sum_{I_g}\delta(I_rI_bI_g-1),$$
$$\Delta_c = \prod_l\theta_c^l\ ,\quad \Delta_i^c = \prod_l\Theta_i^{(l)\bar{c}}\Theta_i^{(l)\bar{\bar{c}}}\quad ;\quad c=r,b,g.$$

The upper limits of sums are just implying the constraint in Eq.(17). All expressions in the above parentheses can be restated as a partition function of a classical Ising model. Before that, notice that the index r in the typical expression $\left(\sum_{\{\theta_r^l\}_{l=1}^n}^{\Delta_r=I_r}e^{\frac{k_r}{2}\sum_l J_r^l\theta_r^l}\right)$ is mute since the sum over configuration of θ_r^l's is done first. Other indices b, g as well as i are mute. Since the θ^l is an Ising variable, it is possible to write it as $\theta^l = \tau^l\tau^{l+1}$, which τ^l's are classical spins. So mapping to the classical Ising model provides a tool to have an analytical expression for entropy. The constraints $\Delta_r = +1$ and $\Delta_r = -1$ are also satisfied by considering the periodic or antiperiodic boundary conditions, respectively. Thus,

$$\prod_r\sum_{\{\theta_r^l\}_{l=1}^n}^{\Delta_r=\pm1}e^{\frac{k_r}{2}\sum_l J_r^l\theta_r^l} = \left(\frac{1}{2}\mathcal{Z}_n^{p/a}(k_r,\{J_r^l\})\right)^{\Sigma_A^r}, \quad (20)$$

where $\mathcal{Z}^{p/a}$ is the partition function of the classical Ising model with periodic or antiperiodic boundary conditions. The partition function of the Ising model can be calculated using the transfer matrix[1] T_l as $\mathcal{Z} = \mathrm{Tr}[\sigma_x^{p/a}\prod_{l=1}^n T_l]$, where σ_x is the usual x-component of the Pauli matrices and $p/a = 0/1$ depending on whether we are considering the periodic or antiperiodic boundary conditions. The corresponding partition function is

$$\mathcal{Z}_n^{p/a} = 2^n\left[\sinh^n(\frac{k_r}{2})\pm\left(\prod_{l=1}^n J_r^l\right)\cosh^n(\frac{k_r}{2})\right]. \quad (21)$$

The partition function related to the green and blue plaquettes have similar forms. One needs only replace the index r by g or b. The expression in the last parenthesis in Eq.(19), which is related to the collective strings, can also be mapped into a partition function. But, the situation is rather tricky. The point is that the terms $\Theta^{(l)g}\Theta^{(l)b}$, $\Theta^{(l)r}\Theta^{(l)g}$ and $\Theta^{(l)b}\Theta^{(l)r}$ are not all independent. So, it is not possible to split the exponential function into three

independent terms and then map each term to a partition function. However, we can use the idea of mapping and transfer matrix. In fact, in this case we use two sets of Ising spins. Let choose τ, s and π as Ising spins. Setting $\Theta^{(l)g}\Theta^{(l)b} = \tau^l\tau^{l+1}$, $\Theta^{(l)r}\Theta^{(l)g} = s^l s^{l+1}$ and $\Theta^{(l)b}\Theta^{(l)r} = \pi^l\pi^{l+1}$ subject to the constraint $\tau^l\tau^{l+1}s^l s^{l+1}\pi^l\pi^{l+1} = 1$, we hope to calculate the following partition function. Notice that there are a 4-1 mapping between Ising spins and colored strings.

$$\mathcal{Z}\left(k_r\Sigma_i^r, k_b\Sigma_i^b, k_g\Sigma_i^g; \{J_r^l\}, \{J_b^l\}, \{J_g^l\}\right) = \sum_{\{\tau^l, s^l, \pi^l\}}^{const.} e^{\sum_l \left(\frac{k_r}{2}J_r^l\Sigma_i^r\tau^l\tau^{l+1} + \frac{k_b}{2}J_b^l\Sigma_i^{(l)b}s^l s^{l+1} + \frac{k_g}{2}J_g^l\Sigma_i^g\pi^l\pi^{l+1}\right)}. \tag{22}$$

First, consider the case with constraints $\Delta_i^c = 1$ for $c = r, b, g$. The transfer matrix will be a 4×4 matrix as follows:

$$T_l = \begin{pmatrix} e^{J_b^l\mathbf{b}+J_g^l\mathbf{g}+J_r^l\mathbf{r}} & e^{-J_b^l\mathbf{b}-J_g^l\mathbf{g}+J_r^l\mathbf{r}} & e^{J_b^l\mathbf{b}-J_g^l\mathbf{g}-J_r^l\mathbf{r}} & e^{-J_b^l\mathbf{b}+J_g^l\mathbf{g}-J_r^l\mathbf{r}} \\ e^{-J_b^l\mathbf{b}+J_g^l\mathbf{g}-J_r^l\mathbf{r}} & e^{J_b^l\mathbf{b}+J_g^l\mathbf{g}+J_r^l\mathbf{r}} & e^{-J_b^l\mathbf{b}-J_g^l\mathbf{g}+J_r^l\mathbf{r}} & e^{J_b^l\mathbf{b}-J_g^l\mathbf{g}-J_r^l\mathbf{r}} \\ e^{J_b^l\mathbf{b}-J_g^l\mathbf{g}-J_r^l\mathbf{r}} & e^{-J_b^l\mathbf{b}+J_g^l\mathbf{g}-J_r^l\mathbf{r}} & e^{J_b^l\mathbf{b}+J_g^l\mathbf{g}+J_r^l\mathbf{r}} & e^{-J_b^l\mathbf{b}-J_g^l\mathbf{g}+J_r^l\mathbf{r}} \\ e^{-J_b^l\mathbf{b}-J_g^l\mathbf{g}+J_r^l\mathbf{r}} & e^{J_b^l\mathbf{b}-J_g^l\mathbf{g}-J_r^l\mathbf{r}} & e^{-J_b^l\mathbf{b}+J_g^l\mathbf{g}-J_r^l\mathbf{r}} & e^{J_b^l\mathbf{b}+J_g^l\mathbf{g}+J_r^l\mathbf{r}} \end{pmatrix}, \tag{23}$$

where $\mathbf{b} = \frac{k_b}{2}\Sigma_i^b$, $\mathbf{g} = \frac{k_g}{2}\Sigma_i^g$ and $\mathbf{r} = \frac{k_r}{2}\Sigma_i^r$. The eigenvalues of the transfer matrix can be easily calculated. Let us denote them by $\xi_{1i}^b = 4J_b^l\xi_{1i}$, $\xi_{2i}^g = 4J_g^l\xi_{2i}$, $\xi_{3i}^r = 4J_r^l\xi_{3i}$ and $4\xi_{4i}$, where

$$\begin{aligned}
\xi_{1i} &= \frac{1}{2}e^{\mathbf{b}}\cosh(\mathbf{g}+\mathbf{r}) - \frac{1}{2}e^{-\mathbf{b}}\cosh(\mathbf{g}-\mathbf{r}) \\
\xi_{2i} &= \frac{1}{2}e^{\mathbf{g}}\cosh(\mathbf{b}+\mathbf{r}) - \frac{1}{2}e^{-\mathbf{g}}\cosh(\mathbf{b}-\mathbf{r}) \\
\xi_{3i} &= \frac{1}{2}e^{\mathbf{r}}\cosh(\mathbf{b}+\mathbf{g}) - \frac{1}{2}e^{-\mathbf{r}}\cosh(\mathbf{b}-\mathbf{g}) \\
\xi_{4i} &= \frac{1}{2}e^{\mathbf{b}}\cosh(\mathbf{g}+\mathbf{r}) + \frac{1}{2}e^{-\mathbf{b}}\cosh(\mathbf{g}-\mathbf{r}).
\end{aligned} \tag{24}$$

Thus, regarding the constraints $\Delta_i^c = 1$ for $c = r, b, g$ that are indicated by the superscript *ppp* in the following expression, the partition function reads as follows:

$$\mathcal{Z}_n^{ppp} = 4^n\left[J_b\xi_{1i}^n + J_g\xi_{2i}^n + J_r\xi_{3i}^n + \xi_{4i}^n\right], \tag{25}$$

where the simplification $J_c = \prod_{l=1}^n J_c^l$ has been used. Considering other constraints that amount to applying the antiperiodic boundary conditions on Ising spins, the sings of J_c in the above expression change correspondingly. For example, if we were to consider the $\Delta_i^b = -\Delta_i^g = -\Delta_i^r = 1$, the sings of coefficients J_g and J_r become minus. Therefore, other partition functions are as follows:

$$\begin{aligned}
\mathcal{Z}_n^{aap} &= 4^n\left[-J_b\xi_{1i}^n + J_g\xi_{2i}^n - J_r\xi_{3i}^n + \xi_{4i}^n\right], \\
\mathcal{Z}_n^{paa} &= 4^n\left[-J_b\xi_{1i}^n - J_g\xi_{2i}^n + J_r\xi_{3i}^n + \xi_{4i}^n\right], \\
\mathcal{Z}_n^{apa} &= 4^n\left[J_b\xi_{1i}^n - J_g\xi_{2i}^n - J_r\xi_{3i}^n + \xi_{4i}^n\right].
\end{aligned} \tag{26}$$

Thus, the expression in Eq.(19) is entirely given in terms of partition functions studied here as follows:

$$\begin{aligned}
\mathrm{Tr}[\rho_A^n] \;=\; & \left(\frac{d_B}{|G|}\right)^{n-1} \frac{1}{4^{2n} Z_0^n} \frac{1}{2^{\Sigma_A+2m_B}} \sum_{\{J_r^l\}_{l=1}^n} \sum_{\{J_b^l\}_{l=1}^n} \sum_{\{J_g^l\}_{l=1}^n} \left[\prod_{l=1}^n \delta\left(J_r^l J_b^l J_g^l - 1\right)\right] \times \\
& \Bigg\{ \left(\mathcal{Z}_n^{(p)}(k_r,\{J_r^l\})\right)^{\Sigma_A^r} \left(\mathcal{Z}_n^{(p)}(k_b,\{J_b^l\})\right)^{\Sigma_A^b} \left(\mathcal{Z}_n^{(p)}(k_g,\{J_g^l\})\right)^{\Sigma_A^g} \prod_i \mathcal{Z}_n^{ppp}(k_r\Sigma_i^r, k_b\Sigma_i^b, k_g\Sigma_i^g; \{J_r^l\},\{J_b^l\},\{J_g^l\}) \\
& + \left(\mathcal{Z}_n^{(a)}(k_r,\{J_r^l\})\right)^{\Sigma_A^r} \left(\mathcal{Z}_n^{(a)}(k_b,\{J_b^l\})\right)^{\Sigma_A^b} \left(\mathcal{Z}_n^{(p)}(k_g,\{J_g^l\})\right)^{\Sigma_A^g} \prod_i \mathcal{Z}_n^{aap}(k_r\Sigma_i^r, k_b\Sigma_i^b, k_g\Sigma_i^g; \{J_r^l\},\{J_b^l\},\{J_g^l\}) \\
& + \left(\mathcal{Z}_n^{(p)}(k_r,\{J_r^l\})\right)^{\Sigma_A^r} \left(\mathcal{Z}_n^{(a)}(k_b,\{J_b^l\})\right)^{\Sigma_A^b} \left(\mathcal{Z}_n^{(a)}(k_g,\{J_g^l\})\right)^{\Sigma_A^g} \prod_i \mathcal{Z}_n^{paa}(k_r\Sigma_i^r, k_b\Sigma_i^b, k_g\Sigma_i^g; \{J_r^l\},\{J_b^l\},\{J_g^l\}) \\
& + \left(\mathcal{Z}_n^{(a)}(k_r,\{J_r^l\})\right)^{\Sigma_A^r} \left(\mathcal{Z}_n^{(p)}(k_b,\{J_b^l\})\right)^{\Sigma_A^b} \left(\mathcal{Z}_n^{(a)}(k_g,\{J_g^l\})\right)^{\Sigma_A^g} \prod_i \mathcal{Z}_n^{apa}(k_r\Sigma_i^r, k_b\Sigma_i^b, k_g\Sigma_i^g; \{J_r^l\},\{J_b^l\},\{J_g^l\}) \Bigg\},
\end{aligned} \tag{27}$$

where $\Sigma_A = \Sigma_A^r + \Sigma_A^b + \Sigma_A^g$. The sum over J_c^l's can be easily taken. Notice $J_c = \pm 1$. Due to the delta function, this leads to $J_r J_b J_g = 1$. So, in summation the $\mathrm{Z}_2 \times \mathrm{Z}_2$ symmetry is automatically held. Therefore, the factors $J_c = \prod_{l=1}^n J_c^l$ in the above expression can be safely dropped since the mentioned symmetry get simply exchanged the terms between brackets. The sums give a multiplicative factor $(\frac{1}{2} \times 8)^n$, where the coefficient $\frac{1}{2}$ arises because of the delta function. It is convenient to introduce the notations $x_c = \cosh(\frac{k_c}{2})$ and $y_c = \sinh(\frac{k_c}{2})$. By inserting Eq.(21), Eq.(25) and Eq.(26) into Eq.(27), we eventually arrive at the following expression.

$$\begin{aligned}
\mathrm{Tr}[\rho_A^n] \;=\; & \frac{1}{4Z_0}\left(\frac{d_A d_B}{Z_0|G|}\right)^{n-1} \times \\
& \left(F_1^{(n)} + F_2^{(n)} + F_3^{(n)} + F_4^{(n)}\right),
\end{aligned} \tag{28}$$

where F's are functions of x_c, y_c and ξ's (see Appendix(X A)). In particular, the replica trick gives the entanglement entropy as follows

$$\begin{aligned}
S_A(T) \;=\; & -\ln\left(\frac{d_A d_B}{|G|}\right) + \ln(Z_0) \\
& -\frac{1}{4Z_0}\left(\partial F_1 + \partial F_2 + \partial F_3 + \partial F_4\right),
\end{aligned} \tag{29}$$

where ∂F's are given in Appendix(X A). This relation is at the heart of our subsequent discussions.

V. LIMITING BEHAVIOR OF ENTANGLEMENT ENTROPY AND MUTUAL INFORMATION

Eq.(29) gives all we need to explore the dependency of entanglement entropy on temperature since apart from the first term the remaining ones depend on temperature. First, suppose the size of the system is finite. As the temperature goes to zero, all terms that depend on temperature vanish and the entanglement entropy of ground state is recovered[27]. The zero-temperature entropy is $S_A(T \to 0) = -\ln(\frac{d_A d_B}{|G|})$. High-temperature limit of the model corresponds to a classical model captured through the "hard constrained limit". As the temperature tends to infinity, the couplings $k_c \to \infty$ leading to $x_c \sim y_c \sim \frac{1}{2}e^{k_c/2}$ and $\xi_{1i} \sim \xi_{2i} \sim \xi_{3i} \sim \xi_{4i} \sim \frac{1}{4}e^{\mathbf{b}+\mathbf{r}+\mathbf{g}}$. At this limit the entanglement entropy acquires a contribution from the bulk degrees of freedom of region A as follows

$$S_A(T \to \infty) = (\Sigma_{AB} + \Sigma_A - 2m_A)\ln 2. \tag{30}$$

This is expected in the sense that at high-temperature limit the thermal entropy that scales with the volume of the region must be reached. This also verifies that the extension of von Neumann entropy to finite temperatures makes sense, since it contains a bulk contribution (scaling with the volume of subsystem A) that corresponds to the ordinary classical entropy. However, the above entropy, despite being at high temperature limit, carries a constant term. This term $2m_A$ depends only on the topology of the region A. This exhibits even at high temperature limit the underlying system may carry topological order. Here,the classical system is constructed by thermalization of a pure density matrix via the high constrained limit[29]. In this way precisely half of the original topological order is preserved at the classical limit. We will refer to this point in next section where the topological entanglement entropy as a measure of the topological order is calculated.

Now, we turn on to take first the thermodynamic limit. In this limit, the entanglement entropy behaves as

$$\begin{aligned}
S_A(T) \;=\; & -\ln\left(\frac{d_A d_B}{|G|}\right) + \frac{N}{2}(k_r + k_b + k_g) - \ln(4) \\
& -e^{-\frac{N}{2}(k_r+k_b+k_g)}\left(\partial F_1 + \partial F_2 + \partial F_3 + \partial F_4\right).
\end{aligned} \tag{31}$$

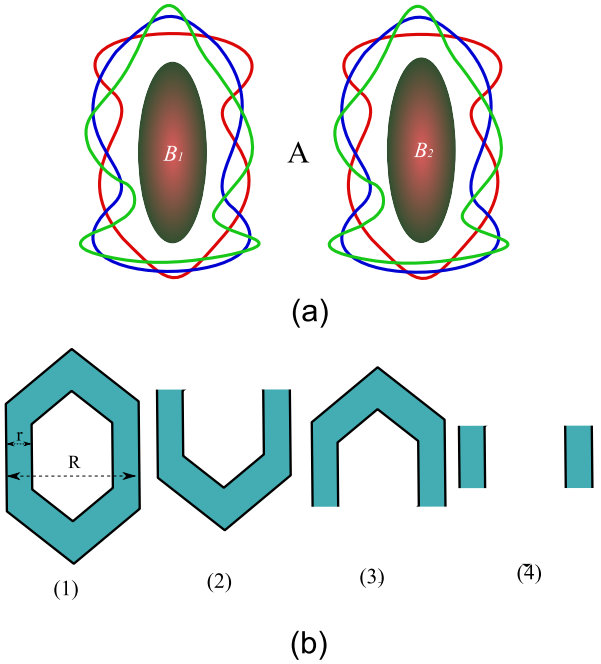

FIG. 2: (color online) (a) A schematic representation of simple connected region A and two disjoint regions B_1 and B_2. For each disjoint region we can realize three colored collective strings: blue(dark gray), red(gray) and green(light gray). All of them are not independent as in text. (b) A set of bipartitions of the lattice in different manner in which all bulk and boundary contribution are dropped through the definition of the topological entropy.

It is simple to check that in the thermodynamic limit $\partial F_2, \partial F_3, \partial F_4$ tend to zero, and the above expression becomes

$$\begin{aligned} S_A(T) &= -\ln\left(\frac{d_A d_B}{|G|}\right) + \frac{N}{2}(k_r+k_b+k_g) - \ln(4) \\ &- \sum_c \left(e^{k_c/2}(x_c \ln x_c + y_c \ln y_c) - \frac{k_c}{2}\right) \\ &- \sum_i e^{-\frac{k_r}{2}\Sigma^r_{p_i} - \frac{k_b}{2}\Sigma^b_{p_i} - \frac{k_g}{2}\Sigma^g_{p_i}} \Big(\xi_{1i}\ln\xi_{1i} \\ &+ \xi_{2i}\ln\xi_{2i} + \xi_{3i}\ln\xi_{3i} + \xi_{4i}\ln\xi_{4i}\Big). \end{aligned} \tag{32}$$

To have a more intuitive picture of above expression, let us consider the limit of large bipartitions which amount to $\Sigma^c_A, \Sigma^c_{p_i} \gg 1$. Finally, we are left with the following expression for the entanglement entropy

$$\begin{aligned} S_A(T)_{N\to\infty} &= (\Sigma_{AB} - 2m_A)\ln 2 \\ &- \sum_c \left[e^{k_c/2}(x_c \ln x_c + y_c \ln y_c) - \frac{k_c}{2}\right]\Sigma^c_A. \end{aligned} \tag{33}$$

If the high-temperature limit is taken, the result coincides with Eq.(30). However, the result is not consistent with the zero-temperature limit. That which limit is taken first would affect the entanglement entropy as

$$\begin{aligned} \lim_{T\to 0, N\to\infty} S_A &= (\Sigma_{AB} - 2m_A)\ln 2, \\ \lim_{N\to\infty, T\to 0} S_A &= (\Sigma_{AB} - 2m_A - 2m_B + 2)\ln 2. \end{aligned} \tag{34}$$

Both quantities scale with the size of the boundary, i.e. the area law holds no matter which limit is taken first. However, the subleading terms are different. The difference between two quantities is $2(m_B - 1)$, which implies that the difference depends only on the topological properties of the regions. Like the toric code model[31], the topological contribution to the entanglement entropy in the color code can be extracted by a single bipartition of the model, provided the region B be a multicomponent region, i.e. $m_B > 1$.

At zero-temperature the entanglement entropy is symmetric upon the exchange of two subsystems A and B, namely $S_A(0) = S_B(0)$. But, this is no longer true at finite temperature. This is because the entanglement entropy acquires an extensive contribution from the bulk degrees of freedom of the region. At finite temperature the entanglement entropy is not a measure of quantum correlations between subsystems. The relevant quantity that drops the bulk dependency and is symmetric between two subsystems as well is the so called "mutual information". The mutual information grasps the total correlations (quantum and classical) between two subsystems. In particular, it is a linear combination of entanglement entropy as follows

$$\mathcal{I}_{AB}(T) = \frac{1}{2}\left(S_A(T) + S_B(T) - S_{A\cup B}(T)\right). \tag{35}$$

Again, the von Numann entropies for subsystems A and B as well as whole system $A\cup B$ are captured by Eq.(29). Notice that $\Sigma_{A\cup B} = 3N$. The derivation of the mutual information is straitforward. However, its full expression will be lengthy. Instead of given the full expression, we only give the limiting behavior as for the entanglement entropy. For finite size systems, the zero-temperature behavior coincides with the entanglement entropy since at zero-temperature the system will be in a pure state and the entropy $S_{A\cup B}(T)$ vanishes. However, at the high-temperature limit, where the classical description holds, the mutual information is symmetric between two subsystems and scales with boundary supplemented with topological terms as follows.

$$\mathcal{I}_{AB} = \frac{1}{2}\left(\Sigma_{AB} - 2m_A - 2m_B + 2\right)\ln 2. \tag{36}$$

This quantity reveals that in the classical model precisely half of the mutual information at zero-temperature survives. Apart from the boundary term, the remaining terms are topological depending on the topology of the subsystems and underlying topological order manifests

itself through them. Once again, classical system supports half of the topological order of the quantum system at zero-temperature. Taking first thermodynamic limit and then zero-temperature limit don't commute with the opposite case. While both limits scale with the boundary, the contribution of topological terms are different. The topological contribution to the mutual information can be filtered out by taking the difference between two following limits:

$$\begin{aligned}\lim_{T\to 0,N\to\infty}\mathcal{I}_{AB} &= (\Sigma_{AB}-m_A-m_B+1)\ln 2,\\ \lim_{N\to\infty,T\to 0}\mathcal{I}_{AB} &= (\Sigma_{AB}-2m_A-2m_B+2)\ln 2.\end{aligned} \tag{37}$$

The difference

$$\Delta\mathcal{I}_{AB}=\lim_{T\to 0,N\to\infty}\mathcal{I}_{AB}-\lim_{N\to\infty,T\to 0}\mathcal{I}_{AB}$$

depends only on the topology of the regions as $\Delta\mathcal{I}_{AB}=(m_A+m_B-1)\ln 2$. The advantage of this latter relation, in contrast to Eq.(34), is that even a simply connected bipartition of both subsystems give rises to a nonvanishing value. So, the mutual information paves the way in which we can define a purely topological order quantity using a simple connected region, in contrast to linear combination over different bipartitions[19,20].

VI. TOPOLOGICAL ENTANGLEMENT ENTROPY

A. finite values of λ_x^c

Topological entanglement entropy[19,20] appears as a subleading term of the entanglement entropy of a region with its complement in the topological phases. It is proposed that this subleading term can be used as a measure of topological order[38]. In this section we use this measure to evaluate the behavior of topological order versus temperature in the topological color code. Ground state of the color code is appeared as a superposition of two underlying string-net structures. Both of them can be realized on the direct 2-colex lattice (unlike the toric code where one of the loop structure is appeared on the dual lattice). String-net structures are identified by considering the σ^x or σ^z bases. The string-net structure related to the latter bases is preserved by imposing the hard constrained limit. But, the string-net related to the former bases can be evaporated against the temperature. The dependency of the topological entanglement entropy on temperature clarifies how much robust the topological order related to the string-net structure is against the thermal fluctuations. In this subsection we assume that all three couplings λ_x^c are finite.

Thermal fluctuations may be so strong that are able to break the closed strings and leave them with end points. The broken strings as we explained in Sec(II) carry excitations on their end points. Imposing the hard constrained limit on the couplings $\lambda_z^c\to\infty$ in the Hamiltonian in Eq.(1), the appearance of respective excitations is restricted. So, part of topological order related to such strings is preserved. As other couplings, λ_x^c, are finite, one may expect that the thermal fluctuations create the star excitations (See Fig.1) at plaquettes. This means that only excitations with charge (e,χ_c) are created. As we will see the accumulation of these excitations in the model destroys the topological order partially.

As Eq.(29) suggests, the entanglement entropy scales with the boundary as well as bulk degrees of freedom. To get ride of boundary and bulk contribution, it is convenient to use a set of bipartitions, and then a linear combination of their entanglement entropies unveils the topological contribution. This set of bipartitions is shown in Fig.2(b). The following linear combination of four bipartitions gives a purely topological contribution to the entanglement entropy.

$$S_{topo}=\lim_{R,r\to\infty}\left(-S_{1A}+S_{2A}+S_{3A}-S_{4A}\right), \tag{38}$$

where each term is given by the von Neumann entanglement entropy of the corresponding bipartition, R and r are the linear size of the subsystems as shown in Fig.2(b). Large sizes of the regions are taken to make the size of the regions much larger than the correlation length in the topological phase. Notice that with the above bipartitions we have the following identifications for the number of connected and disconnected regions.

$$\begin{aligned}m_{1A}=m_{2A}=m_{3A} &= m_{2B}=m_{3B}=m_{4B}=1,\\ m_{1B} &= m_{4B}=2.\end{aligned} \tag{39}$$

The following relations between number of plaquettes related to different bipartitions also hold.

$$\begin{aligned}\Sigma_{1A}+\Sigma_{4A}&=\Sigma_{2A}+\Sigma_{3A},\\ \Sigma^c_{1A}+\Sigma^c_{1,1}+\Sigma^c_{1,2}&=N,\\ \Sigma^c_{2A}+\Sigma^c_{2,1}&=N,\\ \Sigma^c_{3A}+\Sigma^c_{3,1}&=N,\\ \Sigma^c_{4A}+\Sigma^c_{4,1}&=N.\end{aligned} \tag{40}$$

Notice the ambiguity to the definition of low indices in $\Sigma^c_{j,i}$, where j stands for one of the bipartitions in Fig.2(b) and i has the same meaning as in Eq.(15). The full expression of S_{topo} is very lengthy (see Appendix(X B)). It is rather hard to see the behavior of the topological entanglement entropy versus temperature from this equation. To make this quantity more clear, let us consider some limiting cases. First, we consider the finite size systems. Zero-temperature and high-temperature limits are as follows:

$$\begin{aligned}T\to 0\ (k_c\to 0):&\quad S_{topo}-S_{cc}=0,\\ T\to\infty\ (k_c\to\infty):&\quad S_{topo}-S_{cc}=-2\ln 2,\end{aligned} \tag{41}$$

where $S_{cc} = 4\ln 2$ is the topological entanglement entropy of color code at zero-temperature. In the zero-temperature limit the model coincides with the pure ground state. However, at high-temperature limit, as it is clear from the above relation, precisely half of the topological entropy is removed. This result is obtained along the hard constrained limit that has already been taken. As we discussed in preceding section, one could expect such result. In fact, while in the zero-temperature limit the system is fully topological order, at the hight-temperature limit only the string-net structures related to Z_c plaquettes survive. Since both string-net structures related to X_c and Z_c plaquettes have the same contribution to the topological order of the ground state, destroying one of them give rises to reduction of the topological entanglement entropy by half.

The ground state has topological entropy $S_{cc} = \ln D^2$, where $D = 4$ is the so called quantum dimension of the system. By rising the temperature, the populations of open γ^z string-nets would be favorable since the open strings anticommute with plaquette operators X_c that they share at odd qubits. At the very high temperature limit, $S_{topo}(T \to \infty) = \ln D$ implies that each underlying string-net structure contributes $\ln D$ to the topological entropy of the ground state.

Now, let us comment on whether the thermalization process and taking the classical limit affect the topological sectors of the color code model. The ground state of the color code is 4^{2g}-fold degenerate for the systems that live on a manifold with genus g. The 4^{2g} topological sectors are identified by the eigenvalues of the non-local operators winding the handles of the manifold. These non-local operators are product of σ^z operators along the winding closed string as $\mathcal{S}_\mu^{c,z} = \prod_{i\in\Gamma_\mu^c} \sigma_i^z$, where μ and c stand for homology and color of the respective string and Γ_μ^c is the support of qubits winding the handle. By a closed c-string we mean a set of links that connect c-plaquettes. So, it commutes with all plaquettes. Notice that for each homology class there are three winding strings each of one color. However, because of the interplay between color and homology only two of them are independent. Besides, any other closed strings belonging to the same homology class are equivalent up to a deformation.

Within each sector, the ground state is the equal superposition of all bases obtained by any given state in the sector and applying the plaquette operators as in Eq.(2). For any ground state, the respective totally mixed state that corresponds to the density matrix at high-temperature limit is obtained by removing all non-diagonal elements of pure density matrix. The value of non-local string operators will be preserved by taking the high-temperature limit. This latter point implies that topological sectors are not get mixed through the thermalization of the code. In fact, for any mixed density matrix, the expectation value of the any closed non-winding loops that are product of plaquette operators will be +1 in the hard constrained system. Classically changing the topological sectors by flipping the spins along winding loops are exponentially suppressed leading to the so-called broken ergodicity[29], where the phase space is divided into topological sectors.

What happens if we take the thermodynamic limit first? As the size of the system goes to infinity, all $\Sigma_{j,i}^c$ tends to infinity except one $\Sigma_{1,1}^c$ related to the inner region of Fig.2(b(1)). Thus, the expression in Ap-

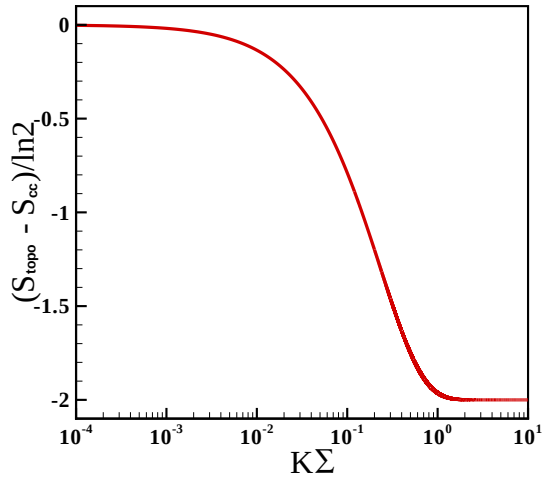

FIG. 3: (color online) Variation of topological entanglement entropy in terms of coupling $K\Sigma$. The horizontal axis is in the logarithmic scales.

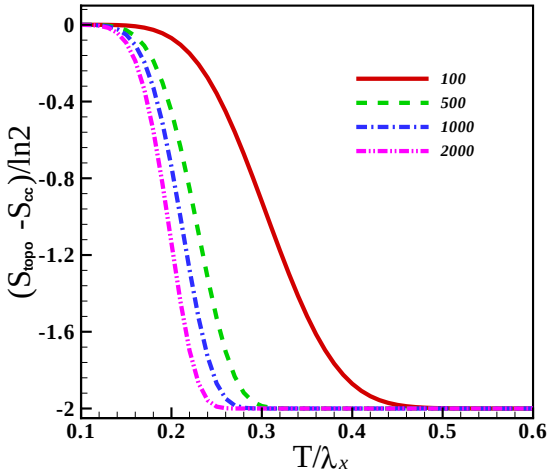

FIG. 4: (color online) Variation of the topological entanglement entropy in terms of temperature. Different curves correspond to different sizes of the inner bipartition in Fig.2(b(1)). In the limit of high temperatures all topological entropy vanishes.

pendix(X B) gets more simplified as follows:

$$S_{topo}\ (T)\ -S_{cc}(0) \rightarrow^{N\rightarrow\infty} \Big\{ e^{-\frac{k_r}{2}\Sigma^r_{1,1}-\frac{k_b}{2}\Sigma^b_{1,1}-\frac{k_g}{2}\Sigma^g_{1,1}} \times (\xi^{(1)}_{11}\ln\xi^{(1)}_{11} + \xi^{(1)}_{21}\ln\xi^{(1)}_{21} + \xi^{(1)}_{31}\ln\xi^{(1)}_{31} + \xi^{(1)}_{41}\ln\xi^{(1)}_{41}) \Big\} - \frac{k_r}{2}\Sigma^r_{1,1} - \frac{k_b}{2}\Sigma^b_{1,1} - \frac{k_g}{2}\Sigma^g_{1,1}. \quad (42)$$

To get more intuitive picture of above relation, we plot the variation of $S_{topo}(T) - S_{cc}(0)$ in terms of $K\Sigma$ and temperature in Fig.(3) and Fig.(4), respectively. For simplicity we have set $K = k_c$ and $\Sigma = \Sigma^c_{1,1}$. For finite size partition, the topological entropy drops as long as the temperature increases. However, even at the high-temperature limit half of topological entropy survives due to the hard constrained limit. As it is clear in Fig.3 at $K\Sigma = \frac{1}{10}$, a drop occurs at topological entropy. We use this to estimate a characteristic temperature above which the topological order disappears. The approximate temperature reads as follows:

$$T_{drop} \simeq \frac{\lambda_x}{\ln(\sqrt{2\Sigma'})}, \quad (43)$$

where $\Sigma' = 3\Sigma$ is the total number of plaquettes in the inner region of Fig.2(b(1)). Thus, we can conclude that the dropping temperature depends on both coupling λ_x and size of the partition. When the size of the partition becomes large, the dropping temperature tends to smaller values. This is transparent from Fig.4 where the dropping of the topological entropy versus temperature for different sizes of partition has been plotted. Since we are considering the large sizes of the partition in the very definition of the entanglement entropy, it is natural to consider the limit of $\Sigma \gg 1$ in Eq.(42) that amounts to the following relation:

$$S_{topo}\ (T)\ -S_{cc}(0) \rightarrow^{N\rightarrow\infty} -2\ln 2, \quad (44)$$

which explicitly implies that in the thermodynamic limit the topological entropy is fragile at any non-zero temperature. This is also expected from the dropping temperature if the bipartitions grow proportional to each other. By this we mean that each bipartition scales by a coefficient proportional to the size of the system. For instance, for the bipartitions in Fig.2(b(1)), we can write $\Sigma^c_A = \gamma_A N$ and $\Sigma^c_i = \gamma_i N$, where $0 < \gamma < 1$ and $\gamma_A + \gamma^c_1 + \gamma^c_2 = 1$. With this identification, now, we can rewrite the dropping temperature in terms of size of the system as follows:

$$T_{drop} \simeq \frac{\lambda_x}{\ln(\sqrt{N})}, \quad (45)$$

which clearly shows that as the thermodynamic limit is reached, the dropping temperature tends to zero. In the thermodynamic limit only at zero temperature the topological order entirely exists.

B. finite values of λ^c_x but $\lambda^{\bar{c}}_x$, $\lambda^{\bar{\bar{c}}}_x \rightarrow \infty$

Thus far, we have considered all λ^c_x's are finite implying that excitations are allowed in all plaquettes by rising the temperature. As we derived in preceding subsection, at the high temperature limit precisely half of the topological entanglement entropy vanishes. In fact, the string-net structures related to the three colored strings are evaporated and excitations in all plaquettes are favorable. In the ground state, the string-net structures contribute $2\ln D$ to the topological entropy. Now, a question arises. How does an individual colored string impact on the topological entropy? We give an answer to this question in what follows. To do so, we allow for excitations to occur only on c-plaquettes while excitations on other $\bar{c}$- and $\bar{\bar{c}}$-plaquettes are restricted due to the energy cost. This can be done by applying a similar hard constrained limit on the couplings $\lambda^{\bar{c}}_x$ and $\lambda^{\bar{\bar{c}}}_x$ in the Hamiltonian of Eq.(1). Let $c = g$, $\bar{c} = r$ and $\bar{\bar{c}} = b$. Thus, thermal fluctuations produce only open green strings carrying topological charges (e, χ_g). The low lying states of the system are $|\psi[\gamma^z_g]\rangle = \gamma^z_g|\psi\rangle$, where γ^z_g is an arbitrary open green string. Within these states, red and blue plaquettes are vortex free since $[X_r, \gamma^z_g] = 0$ and $[X_b, \gamma^z_g] = 0$.

Taking the limits $\lambda^r_x, \lambda^b_x \rightarrow \infty (k_r, k_b \rightarrow 0)$, the topological entanglement in Eq.(42) behaves as

$$S_{topo}\ (T)\ -S_{cc}(0) \rightarrow^{N\rightarrow\infty} \Big\{ e^{-\frac{k_g}{2}\Sigma^g_{1,1}} \Big[(\cosh\frac{k_g}{2}\Sigma^g_{1,1})\ln(\cosh\frac{k_g}{2}\Sigma^g_{1,1}) + (\sinh\frac{k_g}{2}\Sigma^g_{1,1})\ln(\sinh\frac{k_g}{2}\Sigma^g_{1,1}) \Big] \Big\} - \frac{k_g}{2}\Sigma^g_{1,1}. \quad (46)$$

As we are eventually interested in large sizes of the bipartitions, i.e. $\Sigma^g_{1,1} \gg 1$, any non-zero temperature subsides the topological entanglement as follows

$$S_{topo}\ (T)\ -S_{cc}(0) \rightarrow^{N\rightarrow\infty} -\ln 2. \quad (47)$$

For finite size partitions and in the high-temperature limit, as long as $\lambda^{r,b}_x/T \gg 1$, the same reduction in the topological entropy occurs. It is obvious from the relation in Eq.(47) that with disruption of one type of strings, say green, topological order vanishes partially. This is not same as in Eq.(44), where all closed colored strings are allowed to evaporate.

In order to understand the dependency of the topological entropy to the colored strings, let us consider the non-local winding string operators as order parameters. They are products of pauli operators along paths winding the torus as $\mathcal{S}^{c,x}_\mu = \prod_{i\in\Gamma^c_\mu}\sigma^x_i$. Consider the ground state of the system in the σ^x_i bases. The excited states are then $|\psi[\gamma^z_g]\rangle = \gamma^z_g|\psi\rangle$. If a non-local string and an open green string γ^z_g cross each other odd times and have different colors then $\{\mathcal{S}^{c,x}_\mu, \gamma^z_g\} = 0$. Otherwise they commute. At

the ground state level, the expectation values of non-local strings are nonzero and independent of any deformation of the strings, i.e. $\Upsilon^c(0) = \langle\psi|\mathcal{S}_\mu^{c,x}|\psi\rangle = +1(-1)$, depending on the topological sector we are analyzing it. But, at finite temperature the expectation value is replaced by thermal average as $\Upsilon^c(T) = \frac{1}{N_\Gamma}\sum_{\{\Gamma\}}\langle\mathcal{S}_\mu^{c,x}\rangle_T$. The excitations carrying by open green strings are deconfined and the expectation value of two non-local red (blue) strings on opposite sides of excitations are different. For instance consider an open green string carrying star excitations on its ends as shown in Fig.5(a). The winding blue and red strings cross the green string either odd times (solid wavy lines) or nothing (dashed wavy lines). The solid lines anticommute with green string while dashed lines commute. In the expectation value we must take average over all possible cases. So at finite temperature, the emerging excitations destroy the non-local order parameter $\Upsilon^{r,b}(T) \simeq 0$. However, the expectation value of a non-local green string remains finite since it commutes with defects. These lead to destroying the string-net structure of the ground state through the thermalization. The thermal states still contain closed green strings since they commute with defects, i.e. $[\Lambda_g^x, \gamma_g^z] = 0$, where Λ_g^x is an arbitrary product of σ^x operators living on a closed green string. Notice that closed green strings are product of red and blue plaquettes X_r and X_b for which the expectation values with respect to thermal states are $+1$, i.e. they are stabilized by red and blue plaquettes. Thus, one may expect that the topological order in σ^x bases is partially preserved. This is just the message of the Eq.(47) that topological entanglement entropy can be reexpressed into $S_{topo} = \ln D + \frac{1}{2}\ln D$, where $\ln D$ is due to the string-net structure related to the σ^z bases and $\frac{1}{2}\ln D$ is ascribed to one type of closed colored strings (here green) in σ^x bases survived even at finite temperature.

It is tempting to infer that each colored string contribute $\frac{1}{2}\ln D$ to the topological entropy. However, the string structure of the topological order in the ground state of the color code is subject to the $\mathbf{Z_2} \times \mathbf{Z_2}$ gauge symmetry. This is a property of the color code that each colored string is a $\mathbf{Z_2}$ gauge degrees of freedom, but all strings form a $\mathbf{Z_2} \times \mathbf{Z_2}$ gauge structure that is rooted in the string-net structure of the model. Nature of the topological order in the ground state comes from the fact that the ground state is invariant not only under deformation of strings but also the splitting of a c-string into $\bar{c}$- and $\bar{\bar{c}}$-strings as shown in Fig.5(b). The latter point about splitting corresponds to the structure of the gauge group of the color code as we explained in Sec.(II).

The relation between topological entropy and colored strings can be further understood if we soften more couplings. For example let λ_x^g, λ_x^r be finite while $\lambda_x^b/T \gg 1$. Now, the creation of defects in green and red plaquettes becomes favorable. Although the blue plaquettes remain immune against the thermal fluctuations, the average value of all colored winding strings vanishes, since they anticommute with green or red defects. Thus, all

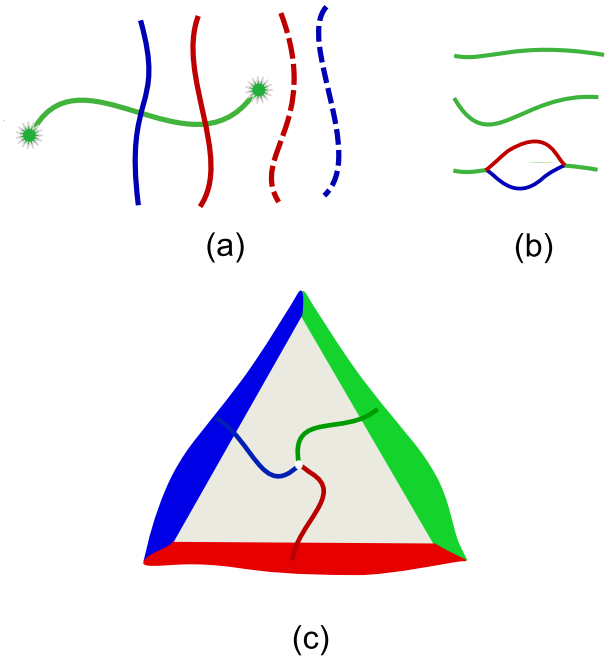

FIG. 5: (color online) (a) An open green (light gray) string carrying star excitations on its ends. The winding blue(dark gray) and red(gray) wavy lines on either sides of the excitation pick up different values. (b) From top to bottom: a colored string, here green, can be either deform or split into red and blue strings. (c) A manifestation of a 2-colex with boundary. Here, we consider a triangular code with three borders: blue(dark gray), red(gray) and green(light gray). A basis for this code is a string-net in which each string has an end point at the border with same color.

topological order vanishes. This can also be seen from the Eq.(42) by letting $\lambda_x^b/T \gg 1(k_b \to 0)$. In the limit of large bipartitions, all topological order vanishes as follows

$$S_{topo}\ \ (T)\ \ -S_{cc}(0) \to^{N\to\infty} -2\ln 2. \qquad (48)$$

Once again when two colored strings are allowed to evaporate, the topological order in the system subsides. Putting all things together, we can conclude that the topological entanglement entropy related to the string-net structure in the σ^x bases receives contributions from the colored strings. In fact, each colored string contributes $\frac{1}{2}\ln D$ to the topological entropy, but the symmetry of the color code model gives rise to the total contribution $2 \times \frac{1}{2}\ln D$.

VII. OPEN BOUNDARY CONDITIONS: PLANAR COLORE CODES

Up to this point, we have only considered the system embedded in a closed surface such as torus, i.e. with periodic boundary conditions. However, the physical system must have boundary in which we can confine to a certain

piece of space. It is simple to obtain an open surface from a closed one by removing some plaquettes of the 2-colex. Such lattices are called planar color code. For example, consider a 2-colex embedded on a sphere. In this case the lattice encodes zero qubits, i.e. the ground state subspace is spanned by a single vector. If we remove a single qubit and its three neighboring links and plaquettes, the obtained 2-colex will encode a single qubit. In fact, three missed plaquettes form three colored borders for the lattice, and only strings with the same color of border will have end points on that border. An example of such bordered lattice is shown in Fig.5(c).

The most important class of the planar color code is the so called triangular color code[24]. The triangular code has three colored borders each of one color (See Fig.5(c)). The logical operators are given by a string-net and its deformation in which make a two-dimensional algebra, since the code encodes only a single qubit. Such string-net is crucial in implementation of the Clifford group. The stabilizer group of the code is again given by a set of plaquettes. However, all plaquettes are independent because of boundary, which affect the number of collective operators needed for evaluating of entanglement entropy. Although a 2-colex on closed and open surfaces may represent different properties for the encoding and implementation of quantum information processing, they represent the same entanglement properties as we will see what follows. This is due to the fact that both structures have same symmetry and topological order comes from the string-net structure of the model.

The group element $\tilde{h}$ can be produced only in one way that is the product of some plaquettes. This amounts to consider only one of the terms in Eq.(7) and Eq.(9). This leads to the following simple relation for $\eta_T(\tilde{h})$.

$$\eta_T(\tilde{h}) = e^{-k_g n_g - k_b n_b - k_r n_r}. \tag{49}$$

We can follow the method in Sec(IV) to map the contribution of plaquettes and collective strings in the group element into Ising variables. However, we should take care about the collective strings. Consider two disjoint regions B_1 and B_2 and connected region A as in Fig.2(a), but, on an open surface. Each disjoint region is surrounded by three colored strings in which only two of them are independent. Observe that two colored strings, say red, surrounding regions B_1 and B_2 are independent, in contrast to the closed surface. By this we mean that if γ_i^r be a collective string around the disjoint region B_i, the $\prod_i \gamma_i^r$ is not the product of blue and green plaquettes of region A. Implication of this point arises in the cardinalities of subgroups G_A and G_B.

Since the open boundary conditions establish only one construction for an group element $\tilde{h}$ in terms of plaquette operators, the preceding arguments leading to the expression in Eq.(27) give only the first term as follows:

$$\begin{aligned}\mathrm{Tr}[\rho_A^n] \;=\; & \left(\frac{d_B}{|G|}\right)^{n-1} \frac{1}{Z_1^n} \frac{1}{2^{\Sigma_A+2m_B}} \sum_{\{J_r^l\}_{l=1}^n} \sum_{\{J_b^l\}_{l=1}^n} \sum_{\{J_g^l\}_{l=1}^n} \left[\prod_{l=1}^n \delta\left(J_r^l J_b^l J_g^l - 1\right)\right] \times \\ & \left\{ \left(\mathcal{Z}_n^{(p)}(k_r, \{J_r^l\})\right)^{\Sigma_A^r} \left(\mathcal{Z}_n^{(p)}(k_b, \{J_b^l\})\right)^{\Sigma_A^b} \left(\mathcal{Z}_n^{(p)}(k_g, \{J_g^l\})\right)^{\Sigma_A^g} \prod_i \mathcal{Z}_n^{ppp}(k_r\Sigma_i^r, k_b\Sigma_i^b, k_g\Sigma_i^g; \{J_r^l\}, \{J_b^l\}, \{J_g^l\}) \right\},\end{aligned} \tag{50}$$

where $Z_1 = e^{\frac{N}{2}(k_g+k_b+k_r)}$. In particular, the replica gives the entanglement entropy as

$$S_A(T) \;=\; -\ln\left(\frac{d_A d_B}{|G|}\right) + \ln(Z_1) - \frac{1}{Z_1}\partial F_1. \tag{51}$$

The expression ∂F_1 is given in Appendix(X A).

For finite size systems, taking the zero-temperature limit gives the entanglement entropy of a single bipartition, $m_A = m_B = 1$, in the ground state of the triangular color code, i.e. $S_A^t(0) = (\Sigma_{AB} - 2)\ln 2$, where the upper index t denotes the triangular code. If we were to take first the thermodynamic limit and then the zero- temperature limit, the limits don't commute with each other. The difference between two limits depends only on the topology of the regions as $\Delta S^t = \lim_{T\to 0, N\to\infty} S_A - \lim_{N\to\infty, T\to 0} S_A^t = 2m_B \ln 2$, which implies that the topological contribution to the entanglement entropy can be extracted even by a single bipartition.

Topological entanglement entropy is given by Eq.(38) and the respective bipartitions in Fig.2(b). We should take into account the restriction imposed by boundary. The cardinalities of bipartitions in Fig.2(b(1)) are $d_A = 2^{\Sigma_{1A}+2}$ and $d_B = 2^{\Sigma_{1B}+2}$. The corresponding quantities for bipartitions in Fig.2(b(2)) and Fig.2(b(3)) are $d_A = 2^{\Sigma_{2,3A}}$ and $d_B = 2^{\Sigma_{2,3B}+2}$. Last bipartition in Fig.2(b(4)) yields the cardinalities $d_A = 2^{\Sigma_{4A}}$ and $d_B = 2^{\Sigma_{4B}+4}$. This leads to the topological entropy of triangular color code at zero temperature[27] as $S_{cc}^t = 4\ln 2$, which is similar with that of the periodic boundary conditions.

Finite temperature topological entropy behaves as

what we derived for closed surface. For finite size systems and at high-temperature limit precisely half of the topological entanglement is preserved as $S^t_{topo}(T \to \infty) - S^t_{cc} = -2\ln 2$, which is a consequence of destroying of string-net structure in the σ^x or σ^z bases. If we take first the thermodynamic limit, any non-zero temperature subsides the topological entropy to half of its value at zero temperature.

VIII. CONCLUSIONS

In this work the topological order in a class of two-dimensional topological stabilizer codes, the so called color code, at finite temperature has been addressed. Both closed and open surfaces, where the lattice embedded on, were considered. This is because quasiparticle excitations are different for each embedding. The stabilizer structure of the color code comes from the plaquette operators which can be of X and Z Pauli operators. The plaquettes are labeled by their color and type. The stabilizer group is adjusted into a many-body Hamiltonian in which the coding space is its ground state subspace. The Hamiltonian is supplemented with energy scales such as λ^c_z's and λ^c_x's. The ground state is a string-net condensate. Closed string-nets are collections of colored strings in which no end points are left. Topological order in the ground state of the model arises from the coherent superposition of two string-net structures that can be visualized by adopting the string-nets in σ^z and σ^x bases. This topological order can be characterized by using the topological entanglement entropy that is $2\ln D$ where $D = 4$.

Considering the limit $\lambda^c_z \to \infty$, the exact solution of the model at finite temperature becomes possible. As the temperature is increased, for finite size systems, the topological entropy reduced to $\ln D$. This implies that by thermalization of one of the string-net structures the respective topological order is destroyed. Both string-net structures have equal contribution to topological entropy.

The temperature at which the topological entropy is dropped is a function of both coupling λ_x and size of system as in Eq.(45). This relation can be used to distinguish a length scale for separated defects. It can be recasted into $Ne^{-2\lambda_x/T_{drop}} \simeq 1$. This means that topological order is destroyed when density of defects in the model becomes of order unity as the temperature is increased. Similar behavior observed in the toric code[31]. This interpretation for density of defects allows us to define the respective length scale as $\zeta_x = e^{\lambda_x/T}$. For temperatures well below the dropping temperature $T \ll T_{drop}$, the characteristic length scale is large implying the density of defects $Ne^{-2\lambda_x/T}$ is much less than unity. In this case the thermal defects are not able to shave out the string-net structure of the model and topological order is preserved. As the temperature increases, the density of defects becomes of order unity that destroy the topological order in the system. In the thermodynamic limit and at finite temperature the distance between defects is much less than the system size. Thus at this limit any nonzero temperature can destroy topological order as in Eq.(44). The robustness of the string-net structure in the hard constrained limit can be understood via such identification for distance between defects. In the limit $\lambda_z \to \infty$ the distance between respective defects $\zeta_z = e^{\lambda_z/T}$ is infinity. So, the respective topological order is immune even in the high temperature limit. This is the reason why in the high constrained system half of the topological order is preserved.

Topological order in the color code arises from coherent superposition of string-net structures in σ^x and σ^z bases. Both structures are similar having the same contribution in the topological entropy. By imposing extra conditions on the couplings λ^c_x, we can examine the contribution of colors and underlying symmetry on the topological entropy. If we let for defects to occur only in c-plaquettes, i.e. $\lambda^{\bar{c}}_x, \lambda^{\bar{\bar{c}}}_x \to \infty$, the thermal states still carry topological order in the σ^x bases even at thermodynamic limit as in Eq.(47). However, if we soften the latter condition and let for defects to occur in both c- and $\bar{c}$-plaquettes, i.e. only let $\lambda^{\bar{\bar{c}}}_x \to \infty$, as Eq.(48) suggests topological order is entirely destroyed. These observations reveal that both colors and symmetry determine the topological entropy. In each loop structure, either in σ^x or σ^z bases, string-nets are collections of closed colored strings. Each colored closed string contributes $\frac{1}{2}\ln D$ to the topological entropy. Considering the gauge symmetry of the model, the total contributions of closed colored strings in the topological entropy will be $\ln D$. In the ground state both string-net structures in σ^x and σ^z bases contribute equally yielding the topological entropy as $2\ln D$.

All above results also hold for the case of open boundary conditions. For this case we considered the triangular color code with borders. Although lattices embedded in closed or open surfaces present different properties from the quantum information perspective, they have similar topological order. This is because they have similar gauge symmetry group and consequently same underlying string structure that is reflected in topological entropy.

The topological order in both toric code and color code models in two-dimensional space is fragile against thermal fluctuations in the sense that their underlying structures are one-dimensional objects, i.e. the strings. This fragility limits their capabilities as self-stability codes. The deconfinement of open strings carrying excitations can be restricted by coupling the defects to bosonic fields[39]. Toric code model in three-dimension have a membrane structure that are robust against thermal noises[35]. The color code model can also be generalized to D-dimensional space with branyon and brane-net structures. It is instructive to generalize the approach presented here to color codes based on the D-colexes[8,34] in the sense that they have different underlying objects as physical mechanism for topological order.

IX. ACKNOWLEDGEMENT

I would like to thank A. Langari for fruitful discussions and comments. I would also like to acknowledge M. A. Martin-Delgado and H. Bombin for their useful comments. This work was supported in part by the Center of Excellence in Complex Systems and Condensed Matter (www.cscm.ir).

X. APPENDIX

A. F's expressions and their derivatives

$F_j^{(n)}$'s for $j = 1, 2, 3, 4$ stand for four terms between the two brackets in Eq.(27). By using the partition functions related to plaquettes and strings that are given in Eq.(21), Eq.(25) and Eq.(26), the following relations for $F_j^{(n)}$'s are obtained.

$$
\begin{aligned}
F_1^{(n)} &= (x_r^n + y_r^n)^{\Sigma_A^r}(x_b^n + y_b^n)^{\Sigma_A^b}(x_g^n + y_g^n)^{\Sigma_A^g} \prod_i (\xi_{1i}^n + \xi_{2i}^n + \xi_{3i}^n + \xi_{4i}^n) \\
F_2^{(n)} &= (x_r^n - y_r^n)^{\Sigma_A^r}(x_b^n - y_b^n)^{\Sigma_A^b}(x_g^n + y_g^n)^{\Sigma_A^g} \prod_i (-\xi_{1i}^n + \xi_{2i}^n - \xi_{3i}^n + \xi_{4i}^n) \\
F_3^{(n)} &= (x_r^n + y_r^n)^{\Sigma_A^r}(x_b^n - y_b^n)^{\Sigma_A^b}(x_g^n - y_g^n)^{\Sigma_A^g} \prod_i (-\xi_{1i}^n - \xi_{2i}^n + \xi_{3i}^n + \xi_{4i}^n) \\
F_4^{(n)} &= (x_r^n - y_r^n)^{\Sigma_A^r}(x_b^n + y_b^n)^{\Sigma_A^b}(x_g^n - y_g^n)^{\Sigma_A^g} \prod_i (\xi_{1i}^n - \xi_{2i}^n - \xi_{3i}^n + \xi_{4i}^n)
\end{aligned} \tag{52}
$$

The case $n = 1$ and their derivatives are needed for evaluation of entanglement entropy. So, the above expressions get more simplified as follows:

$$
\begin{aligned}
F_1^{(1)} &= e^{\frac{N}{2}(k_r + k_b + k_g)}, \quad F_2^{(1)} = e^{\frac{N}{2}(-k_r - k_b + k_g)}, \\
F_3^{(1)} &= e^{\frac{N}{2}(k_r - k_b - k_g)}, \quad F_4^{(1)} = e^{\frac{N}{2}(-k_r + k_b - k_g)}.
\end{aligned}
$$

Trivially $Z_0 = \frac{1}{4}(F_1^{(1)} + F_2^{(1)} + F_3^{(1)} + F_3^{(1)})$, and their derivatives at $n = 1$ are

$$
\begin{aligned}
\partial F_1 = (\partial F_1^{(n)}/\partial n)_{n\to 1} &= F_1^{(1)}\Bigg[\Sigma_A^r e^{\frac{-k_r}{2}}(x_r\ln x_r + y_r\ln y_r) + \Sigma_A^b e^{\frac{-k_b}{2}}(x_b\ln x_b + y_b\ln y_b) + \Sigma_A^g e^{\frac{-k_g}{2}}(x_g\ln x_g + y_g\ln y_g) \\
&\quad + \sum_i e^{-\frac{k_r}{2}\Sigma_i^r - \frac{k_b}{2}\Sigma_i^b - \frac{k_g}{2}\Sigma_i^g}(\xi_{1i}\ln\xi_{1i} + \xi_{2i}\ln\xi_{2i} + \xi_{3i}\ln\xi_{3i} + \xi_{4i}\ln\xi_{4i})\Bigg], \\
\partial F_2 = (\partial F_2^{(n)}/\partial n)_{n\to 1} &= F_2^{(2)}\Bigg[\Sigma_A^r e^{\frac{k_r}{2}}(x_r\ln x_r - y_r\ln y_r) + \Sigma_A^b e^{\frac{k_b}{2}}(x_b\ln x_b - y_b\ln y_b) + \Sigma_A^g e^{\frac{-k_g}{2}}(x_g\ln x_g + y_g\ln y_g) \\
&\quad + \sum_i e^{\frac{k_r}{2}\Sigma_i^r + \frac{k_b}{2}\Sigma_i^b - \frac{k_g}{2}\Sigma_i^g}(-\xi_{1i}\ln\xi_{1i} + \xi_{2i}\ln\xi_{2i} - \xi_{3i}\ln\xi_{3i} + \xi_{4i}\ln\xi_{4i})\Bigg], \\
\partial F_3 = (\partial F_3^{(n)}/\partial n)_{n\to 1} &= F_3^{(3)}\Bigg[\Sigma_A^r e^{\frac{-k_r}{2}}(x_r\ln x_r + y_r\ln y_r) + \Sigma_A^b e^{\frac{k_b}{2}}(x_b\ln x_b - y_b\ln y_b) + \Sigma_A^g e^{\frac{k_g}{2}}(x_g\ln x_g - y_g\ln y_g) \\
&\quad + \sum_i e^{-\frac{k_r}{2}\Sigma_i^r + \frac{k_b}{2}\Sigma_i^b + \frac{k_g}{2}\Sigma_i^g}(-\xi_{1i}\ln\xi_{1i} - \xi_{2i}\ln\xi_{2i} + \xi_{3i}\ln\xi_{3i} + \xi_{4i}\ln\xi_{4i})\Bigg], \\
\partial F_4 = (\partial F_4^{(n)}/\partial n)_{n\to 1} &= F_4^{(4)}\Bigg[\Sigma_A^r e^{\frac{k_r}{2}}(x_r\ln x_r - y_r\ln y_r) + \Sigma_A^b e^{\frac{-k_b}{2}}(x_b\ln x_b + y_b\ln y_b) + \Sigma_A^g e^{\frac{k_g}{2}}(x_g\ln x_g - y_g\ln y_g) \\
&\quad + \sum_i e^{\frac{k_r}{2}\Sigma_i^r - \frac{k_b}{2}\Sigma_i^b + \frac{k_g}{2}\Sigma_i^g}(\xi_{1i}\ln\xi_{1i} - \xi_{2i}\ln\xi_{2i} - \xi_{3i}\ln\xi_{3i} + \xi_{4i}\ln\xi_{4i})\Bigg],
\end{aligned}
\tag{53}
$$

B. Topological Entropy

Applying Eq.(29) about each bipartition of Fig.(2b), and inserting into Eq.(38), the topological entanglement entropy then reads as follows:

$$
\begin{aligned}
S_{topo}(T) \;-\; S_{cc}(0) = \\
&\frac{1}{4Z_0}\sum_{i=1}^{2}\Big\{ e^{\frac{k_r}{2}(N-\Sigma^r_{1,i})+\frac{k_b}{2}(N-\Sigma^b_{1,i})+\frac{k_g}{2}(N-\Sigma^g_{1,i})}(\xi^{(1)}_{1i}\ln\xi^{(1)}_{1i}+\xi^{(1)}_{2i}\ln\xi^{(1)}_{2i}+\xi^{(1)}_{3i}\ln\xi^{(1)}_{3i}+\xi^{(1)}_{4i}\ln\xi^{(1)}_{4i}) \\
&+e^{-\frac{k_r}{2}(N-\Sigma^r_{1,i})-\frac{k_b}{2}(N-\Sigma^b_{1,i})+\frac{k_g}{2}(N-\Sigma^g_{1,i})}(-\xi^{(1)}_{1i}\ln\xi^{(1)}_{1i}+\xi^{(1)}_{2i}\ln\xi^{(1)}_{2i}-\xi^{(1)}_{3i}\ln\xi^{(1)}_{3i}+\xi^{(1)}_{4i}\ln\xi^{(1)}_{4i}) \\
&+e^{\frac{k_r}{2}(N-\Sigma^r_{1,i})-\frac{k_b}{2}(N-\Sigma^b_{1,i})-\frac{k_g}{2}(N-\Sigma^g_{1,i})}(-\xi^{(1)}_{1i}\ln\xi^{(1)}_{1i}-\xi^{(1)}_{2i}\ln\xi^{(1)}_{2i}+\xi^{(1)}_{3i}\ln\xi^{(1)}_{3i}+\xi^{(1)}_{4i}\ln\xi^{(1)}_{4i}) \\
&+e^{-\frac{k_r}{2}(N-\Sigma^r_{1,i})+\frac{k_b}{2}(N-\Sigma^b_{1,i})-\frac{k_g}{2}(N-\Sigma^g_{1,i})}(\xi^{(1)}_{1i}\ln\xi^{(1)}_{1i}-\xi^{(1)}_{2i}\ln\xi^{(1)}_{2i}-\xi^{(1)}_{3i}\ln\xi^{(1)}_{3i}+\xi^{(1)}_{4i}\ln\xi^{(1)}_{4i})\Big\} \\
&-\frac{1}{4Z_0}\Big\{ e^{\frac{k_r}{2}(N-\Sigma^r_{2,1})+\frac{k_b}{2}(N-\Sigma^b_{2,1})+\frac{k_g}{2}(N-\Sigma^g_{2,1})}(\xi^{(2)}_{1}\ln\xi^{(2)}_{1}+\xi^{(2)}_{2}\ln\xi^{(2)}_{2}+\xi^{(2)}_{3}\ln\xi^{(2)}_{3}+\xi^{(2)}_{4}\ln\xi^{(2)}_{4}) \\
&+e^{-\frac{k_r}{2}(N-\Sigma^r_{2,1})-\frac{k_b}{2}(N-\Sigma^b_{2,1})+\frac{k_g}{2}(N-\Sigma^g_{2,1})}(-\xi^{(2)}_{1}\ln\xi^{(2)}_{1}+\xi^{(2)}_{2}\ln\xi^{(2)}_{2}-\xi^{(2)}_{3}\ln\xi^{(2)}_{3}+\xi^{(2)}_{4}\ln\xi^{(2)}_{4}) \\
&+e^{\frac{k_r}{2}(N-\Sigma^r_{2,1})-\frac{k_b}{2}(N-\Sigma^b_{2,1})-\frac{k_g}{2}(N-\Sigma^g_{2,1})}(-\xi^{(2)}_{1}\ln\xi^{(2)}_{1}-\xi^{(2)}_{2}\ln\xi^{(2)}_{2}+\xi^{(2)}_{3}\ln\xi^{(2)}_{3}+\xi^{(2)}_{4}\ln\xi^{(2)}_{4}) \\
&+e^{-\frac{k_r}{2}(N-\Sigma^r_{2,1})+\frac{k_b}{2}(N-\Sigma^b_{2,1})-\frac{k_g}{2}(N-\Sigma^g_{2,1})}(\xi^{(2)}_{1}\ln\xi^{(2)}_{1}-\xi^{(2)}_{2}\ln\xi^{(2)}_{2}-\xi^{(2)}_{3}\ln\xi^{(2)}_{3}+\xi^{(2)}_{4}\ln\xi^{(2)}_{4})\Big\} \\
&-\frac{1}{4Z_0}\Big\{ e^{\frac{k_r}{2}(N-\Sigma^r_{3,1})+\frac{k_b}{2}(N-\Sigma^b_{3,1})+\frac{k_g}{2}(N-\Sigma^g_{3,1})}(\xi^{(3)}_{1}\ln\xi^{(3)}_{1}+\xi^{(3)}_{2}\ln\xi^{(3)}_{2}+\xi^{(3)}_{3}\ln\xi^{(3)}_{3}+\xi^{(3)}_{4}\ln\xi^{(3)}_{4}) \\
&+e^{-\frac{k_r}{2}(N-\Sigma^r_{3,1})-\frac{k_b}{2}(N-\Sigma^b_{3,1})+\frac{k_g}{2}(N-\Sigma^g_{3,1})}(-\xi^{(3)}_{1}\ln\xi^{(3)}_{1}+\xi^{(3)}_{2}\ln\xi^{(3)}_{2}-\xi^{(3)}_{3}\ln\xi^{(3)}_{3}+\xi^{(3)}_{4}\ln\xi^{(3)}_{4}) \\
&+e^{\frac{k_r}{2}(N-\Sigma^r_{3,1})-\frac{k_b}{2}(N-\Sigma^b_{3,1})-\frac{k_g}{2}(N-\Sigma^g_{3,1})}(-\xi^{(3)}_{1}\ln\xi^{(3)}_{1}-\xi^{(3)}_{2}\ln\xi^{(3)}_{2}+\xi^{(3)}_{3}\ln\xi^{(3)}_{3}+\xi^{(3)}_{4}\ln\xi^{(3)}_{4}) \\
&+e^{-\frac{k_r}{2}(N-\Sigma^r_{3,1})+\frac{k_b}{2}(N-\Sigma^b_{3,1})-\frac{k_g}{2}(N-\Sigma^g_{3,1})}(\xi^{(3)}_{1}\ln\xi^{(3)}_{11}-\xi^{(3)}_{2}\ln\xi^{(3)}_{2}-\xi^{(3)}_{3}\ln\xi^{(3)}_{3}+\xi^{(3)}_{4}\ln\xi^{(3)}_{4})\Big\} \\
&+\frac{1}{4Z_0}\Big\{ e^{\frac{k_r}{2}(N-\Sigma^r_{4,1})+\frac{k_b}{2}(N-\Sigma^b_{4,1})+\frac{k_g}{2}(N-\Sigma^g_{4,1})}(\xi^{(4)}_{1}\ln\xi^{(4)}_{1}+\xi^{(4)}_{2}\ln\xi^{(4)}_{2}+\xi^{(4)}_{3}\ln\xi^{(4)}_{3}+\xi^{(4)}_{4}\ln\xi^{(4)}_{4}) \\
&+e^{-\frac{k_r}{2}(N-\Sigma^r_{4,1})-\frac{k_b}{2}(N-\Sigma^b_{4,1})+\frac{k_g}{2}(N-\Sigma^g_{4,1})}(-\xi^{(4)}_{1}\ln\xi^{(4)}_{1}+\xi^{(4)}_{2}\ln\xi^{(4)}_{2}-\xi^{(4)}_{31}\ln\xi^{(4)}_{3}+\xi^{(4)}_{4}\ln\xi^{(4)}_{4}) \\
&+e^{\frac{k_r}{2}(N-\Sigma^r_{4,1})-\frac{k_b}{2}(N-\Sigma^b_{4,1})-\frac{k_g}{2}(N-\Sigma^g_{4,1})}(-\xi^{(4)}_{1}\ln\xi^{(4)}_{1}-\xi^{(4)}_{2}\ln\xi^{(4)}_{2}+\xi^{(4)}_{3}\ln\xi^{(4)}_{3}+\xi^{(4)}_{4}\ln\xi^{(4)}_{4}) \\
&+e^{-\frac{k_r}{2}(N-\Sigma^r_{4,1})+\frac{k_b}{2}(N-\Sigma^b_{4,1})-\frac{k_g}{2}(N-\Sigma^g_{4,1})}(\xi^{(4)}_{1}\ln\xi^{(4)}_{1}-\xi^{(4)}_{2}\ln\xi^{(4)}_{2}-\xi^{(4)}_{3}\ln\xi^{(4)}_{3}+\xi^{(4)}_{4}\ln\xi^{(4)}_{4})\Big\},
\end{aligned}
\tag{54}
$$

where $S_{cc}(0)$ stands for the topological entanglement of the color code at zero-temperature, i.e. $S_{cc}(0) = 4\ln 2$. Notice that the upper indices of ξ's are related to the respective bipartitions in Fig.2(b).

References

* kargarian@physics.sharif.edu

[1] N. Goldenfeld, *lectures on phase transitions and the renormalization group*, Westview Press, 1992.

[2] X. G. Wen, *Quantum Field Theory of Many-Body Systems* (Oxford University, New York, 2004).

[3] X.-G. Wen, Int. J. Mod. Phys. B **4**, 239 (1990). X.-G. Wen, Advances in Physics **44**, 405 (1995).

[4] N. Read, Phys. Rev. Lett. **65**, 1502 (1990).

[5] J. Frühlich and T. Kerler, Nucl. Phys. B **354**, 369 (1991).

[6] Michael A. Levin and Xiao-Gang Wen, Phys. Rev. B. **71**, 045110 (2005).

[7] Alioscia Hamma, Paolo Zanardi, and Xiao-Gang Wen, Phys. Rev. B. **72**, 035307 (2005).

[8] H. Bombin and M. A. Martin-Delgado, Phys. Rev. B **75**, 075103 (2007)

[9] F. A. Bais, and J.K.Slingerland, arXiv: 0808.0627.

[10] Michael A. Levin and Xiao-Gang Wen, Phys. Rev. B. **67**, 245316 (2003).

[11] E. Dennis, A. Kitaev, A. Landahl, and J. Preskill, J. Math. Phys. (N.Y.) **43**, 4452 (2002).

[12] R. Alicki, M. Fannes and M. Horodecki, arXiv: 0810.4584.

[13] Zohar Nussinov and Gerardo Ortiz, Phys. Rev. B **77**,

064302 (2008).
[14] A.Yu. Kitaev, Ann. Phys. (N.Y.) 303, **2** (2003).
[15] M. Freedman, M. Larsen, Z. Wang, Comm.Math. Phys. **227** 605, (2002).
[16] M. H. Freedman, A. Kitaev, M. J. Larsen, Z. Wang, Bull. Amer. Math. Soc. **40**, 31 (2003); quant-ph/0101025.
[17] Chetan Nayak, Steven H. Simon, Ady Stern, Michael Freedman, Sankar Das Sarma, arXiv: 0707.1889.
[18] Jiannis K. Pachos, Int. J. Quant. Info, Vol. 4, No. 6 (2006) 947-954.
[19] A. Kitaev and J. Preskill, Phys. Rev. Lett. **96**, 110404 (2006).
[20] M. Levin and X. G. Wen, Phys. Rev. Lett. **96**, 110405 (2006).
[21] J. Eisert, M. Cramer and M.B. Plenio, arXiv: 0808.3773.
[22] A.Yu. Kitaev, Ann. Phys. (N.Y.) 2, **321** (2006).
[23] D. Gottesman, Phys. Rev. A **54**, 1862 (1996).
[24] H. Bombin and M. A. Martin-Delgado, Phys. Rev. Lett. **97**, 180501 (2006).
[25] H. Bombin and M. A. Martin-Delgado, Phys. Rev. A. **76**, 012305 (2007).
[26] H. G. Katzgraber, H. Bombin and M. A. Martin-Delgado, arXiv:0902.4845.
[27] M. Kargarian, Phys. Rev. A. **78**, 062312 (2008).
[28] A. Hamma, R. Ionicioiu, and P. Zanardi, Phys. Rev. A. **71**,022315 (2005); *ibid* Phys. Lett. A **337**, 22 (2005).
[29] Claudio Castelnovo and Claudio Chamon, Phys. Rev. B **76**, 174416 (2007).
[30] S. Iblisdir, D. Perez-Garcia, M. Aguado, and J. Pachos, Phys. Rev. B **79**, 134303 (2009). *ibid* arXiv:0812.4975.
[31] Claudio Castelnovo and Claudio Chamon, Phys. Rev. B **76**, 184442 (2007).
[32] Alastair Kay and Roger Colbeck, arXiv: 0810.3557.
[33] Zohar Nussinov and Gerardo Ortiz, arXiv:0812.4309.
[34] H. Bombin and M. A. Martin-Delgado, Phys. Rev. Lett. **98**, 160502 (2007).
[35] Claudio Castelnovo and Claudio Chamon, Phys. Rev. B **78**, 155120 (2008).
[36] H. Bombin, M. Kargarian and M. A. Martin-Delgado, arXiv:0811.0911.
[37] F.Alexander Bais, Peter van Driel and Mark de Wild Propitius, Phys.Lett. **B280**, 63 (1992).
[38] A. Hamma, W. Zhang, S. Haas, and D. A. Lidar, Phys. Rev. B **77**, 155111 (2008).
[39] Alioscia Hamma, Claudio Castelnovo, and Claudio Chamon, arXiv: 0812.4622.